MULTIPLE QUANTUM TRANSITIONS

MULTIPLE QUANTUM TRANSITIONS

IN

ATOMIC BEAM MAGNETIC RESONANCE

By

ANTON ROBERT PIERCE, B.A.

A Thesis

Submitted to the Faculty of Graduate Studies

in Partial Fulfilment of the Requirements

for the Degree

Master of Science

McMaster University

October 1966

MASTER OF SCIENCE (1966) McMASTER UNIVERSITY
(Physics) Hamilton, Ontario

TITLE: Multiple Quantum Transitions in Atomic Beam Magnetic Resonance

AUTHOR: Anton Robert Pierce, B.A. (Rutgers University)

SUPERVISOR: Dr. R. G. Summers-Gill

NUMBER OF PAGES: vi, 74

SCOPE AND CONTENTS:

The problem of multiple quantum transitions between the magnetic sub-levels of an atomic ground state hyperfine multiplet has been investigated both experimentally and theoretically. Special emphasis has been paid to the behaviour of these transitions as the magnetic sub-levels of the hyperfine multiplet depart from equal level spacing.

The experiments performed determined the power dependence of the multiple quantum transitions of Na^{23}. These experiments led to the establishment of a technique of determining transition multiplicity.

Expressions are also developed which permit the calculation of transition probabilities for arbitrary values of multiplicity, r.f. amplitude and degree of inequality of level spacing.

ACKNOWLEDGEMENTS

It is a pleasure to thank all those who have helped make this work possible. Special thanks must go to the following:

To Dr. R. G. Summers-Gill who originally suggested the problem, developed the theoretical basis for this investigation and provided many useful suggestions during the course of the work.

To Dr. J. A. Cameron for his council and encouragement.

To Dr. M. W. Johns, the chairman of the department, for his kindly discharge of that office.

To the members of the Atomic Beam group, both past and present, G. M. Stinson, J. C. Waddington, A. R. Mufti, R. G. H. Robertson, W. H. Brooker and D. Dohan.

To my mother who taught me that knowledge is sweet.

To my wife, Heather, for her love.

This work was supported by grants to the group from the National Research Council of Canada.

TABLE OF CONTENTS

LIST OF FIGURES

CHAPTER I

INTRODUCTION

A multiple quantum transition (MQT) is a transition in which two or more quanta from an applied electro-magnetic field supply energy and angular momentum to effect the transfer of some system from an initial state to a final state. Such a transition satisfies a generalized Bohr frequency condition

$$E_f - E_i = \pm \hbar\omega_1 \pm \hbar\omega_2 \ldots\ldots \pm \hbar\omega_k \ldots\ldots \qquad (1\text{-}1)$$

where E_i and E_f are the energies of the initial and final states and ω_k is the angular frequency of the k^{th} quantum in the radiation field. There are many instances in physics of such processes -- especially when both absorption and emission are involved. Thus, for example, Raman scattering corresponds to the absorption of one photon and the emission of another. It is a common ingredient of field theory to think of interaction processes going through intermediate states by the absorption and emission of field quanta and the structure of second and higher order perturbation theory suggests this physical picture.

In this work, the term MQT will refer specifically to the case of successive absorption or successive emissions of real photons, and not to mixtures of these processes. Furthermore, consideration will be limited to a monochromatic radiation field so that equation (1) becomes

$$\left| E_f - E_i \right| = n\hbar\omega \qquad (1\text{-}2)$$

and such a transition will be termed an n-quantum transition. Now n = 1

corresponds to a single quantum transition (SQT) but, for the sake of brevity, the term MQT will be used in the inclusive sense of $n \geqslant 1$, and not solely $n > 1$. Within these restrictions, one can further distinguish two limiting cases. Those processes, such as two photon absorption, in which the transition proceeds via a virtual intermediate state occur with only low probability unless the radiation field is very intense. The other case is that where real states exist at the appropriate spacing between initial and final levels. The presence of such levels has a profound effect on the n-quantum transition probability, the more so the more nearly they are located at equal spacing.

Because it is unlikely than any system will have nearly equally spaced optical levels, MQT of the type specified are not observed in optical spectra. Furthermore, spontaneous decay leads to short life-times, and collision processes, etc., depopulate states which would otherwise have longer existence. Thus, only for very intense illumination would there be any significant probability than an intermediate state, once formed, would interact with a second quantum of the external field before "spontaneously" relaxing back to the ground state. In contrast, the weak field Zeeman effect in ground state atomic hyperfine structure leads characteristically to levels that are equally spaced. The small energies involved, and the parity imposed M1 (or E2, etc.) selection rule, essentially eliminate spontaneous emission as a de-excitation process. In a beam type experiment, collisions are also eliminated so that absorption and stimulated emission become the only means of transition. Furthermore, the application of stronger magnetic fields causes the energy levels to

become unequally spaced in a gradual and known way. Thus, the method of atomic beam magnetic resonance (ABMR) is admirably suited for the investigation of MQT.

Indeed, it is because the multiple quantum process is relatively common in ABMR that this study was undertaken. In the determination of the nuclear and electronic parameters which characterize a given atomic species, it is frequently useful, or even essential, to observe and measure the resonance frequencies of MQT. Two examples of this technique have recently been encountered in this laboratory -- the investigation of Sm^{153} (Eastwood, 1964) and Ag^{109m} (Stinson, 1966). In these experiments, transitions were observed that were obviously multiple quantum in nature but the use of their frequencies in elucidating the atomic hyperfine Hamiltonian required knowing or inferring the number of quanta involved. The lack of a definitive means for doing this enforced on these experiments an extensive investigation of the hyperfine structure at a variety of fields and lengthy trial and error calculations before their identity was established with certainty. It would be a great convenience if a simple and direct means could be found for determining the multiplicity of any observed transition. Of course, to be useful in the study of unknown hyperfine structures, it is essential that the method be independent of the degree of departure from equal spacing of the intermediate levels involved.

Atomic beam investigations of the properties of MQT, both theoretical and experimental, have been carried out by a number of workers (Salwen, 1955; Salwen, 1956; Hack, 1956; Kusch, 1956; Franzen and Alam, 1964).

Majorana (Majorana, 1932) calculated MQT transition probabilities for the case of exactly equally spaced levels. In this situation, all MQT occur

at the same frequency. For cases of practical interest in ABMR, this can only occur when the nuclear spin I is zero. (Of course, it is possible to have $I > 0$ and $J = 0$, but then the ABMR technique doesn't apply.) Most observations of MQT in ABMR involve non-zero nuclear spins, so use of the Majorana formula in ABMR is of limited value.

Salwen (Salwen, 1955) and Hack (Hack, 1956) used perturbation theory to calculate MQT transition probabilities. Such approaches via perturbation theory are limited to the case of both small values of r.f. field and to quite unequal spacing of the system's levels, the latter requirement insuring that only a single order of MQT will take place at a given frequency. These requirements, however, constitute conflicting demands; as the levels depart from equal spacing, vastly greater r.f. field amplitudes are required to induce anything but negligibly small MQT probabilities.

Polycarp Kusch (Kusch, 1956) made a detailed comparison between Salwen's theory and experiments he conducted using a beam of K^{39} and a specially designed apparatus which provided extremely homogeneous static magnetic fields. These experiments were performed at one value of magnetic field and, thus, for a single degree of level-splitting. While good agreement resulted for small values of r.f. field amplitudes, discrepancies occurred for large amplitudes. The behaviour of MQT upon the degree of equality of level spacing had yet not been investigated.

In ABMR, a transition's resonance width is severely and non-reproductively widened by inhomogeneities in the magnetic field which produces the Zeeman splitting of the atomic hyperfine multiplet: Kusch's observation, in agreement with the theories of Salwen and Hack, that a MQT resonance line

shape is preferentially narrowed as multiplicity increases, is not a reliable means of identifying the transition multiplicity in the short beam path apparatus used in ABMR experiments on radioactive samples. The trouble is that the over-all shortness of the apparatus requires a short Zeeman magnet and fringing from its end limits field homogeneity. In addition, the over-all apparatus shortness also sandwiches this weak field in between two strong deflecting magnets which have fields fringing into the Zeeman field region to further worry field homogeneity.

Franzen and Alam (Franzen and Alam, 1964) solved exactly the problem for single and double quantum transitions in a system having three levels. The vast majority of cases in ABMR investigations, however, involve systems having more than three levels and the exact results of Franzen and Alam can not be readily utilized.

The body of experimental and theoretical work on MQT, extant at the inception of this investigation, indicated a possible method of finding transition multiplicity in an unknown hyperfine structure. It was known in the limit of exactly equally spaced levels, where the Majorana formula applies, that different order MQT did have markedly and characteristically different dependences upon r.f. field amplitude. The theories of Salwen, Hack and Franzen and Alam also indicated that the power dependence of MQT was greatly altered as transition multiplicity changed. Accordingly, experiments were performed to see if the power dependence of MQT in a beam of Na^{23} could be used to identify the quanticity of the transition involved.

In addition to power dependence experiments, a new formulation of the theory of MQT was developed. A computer programme was written incor-

porating expressions developed in the new theory. Use of an electronic computer permitted MQT probabilities to be exactly calculated for any value of r.f. amplitude and any degree of non-equality of level spacing.

CHAPTER II

GROUND-STATE ATOMIC HYPERFINE STRUCTURE

1. Hyperfine Structure of a Free Atom

In the absence of external fields, the atomic Hamiltonian may be written as:

$$\mathcal{H}_{\text{Atomic}} = \mathcal{H}_{\text{Nuclear}} + \mathcal{H}_{\text{Electronic}} + \mathcal{H}_{\text{Hyperfine}}. \qquad (2\text{-}1)$$

The internal energy of the atomic nucleus is given by $\mathcal{H}_{\text{Nuclear}}$. The term $\mathcal{H}_{\text{electronic}}$ is the Hamiltonian representing the energy of the atom's electrons and their interactions, both electric and magnetic, with the atom's nucleus, on the assumption that this nucleus is a point charge of charge Ze. Thus, it includes terms which take account of the attractive Coulomb force between the atomic electrons and the point charge nucleus, the kinetic energy of the Z electrons, the mutually repulsive Coulomb forces between the Z electrons themselves, and the spin-orbit magnetic interaction. The eigenenergies of $\mathcal{H}_{\text{electronic}}$ give rise to gross atomic spectra and atomic fine structure. The Hamiltonian which gives rise to hyperfine structure, $\mathcal{H}_{\text{Hyperfine}}$, represents electro-magnetic hyperfine interactions other than the mono-pole term between the finite nucleus and the atomic electrons condensed in $\mathcal{H}_{\text{electronic}}$. Physically, the hyperfine interaction couples the nuclear and electronic angular momenta.

Due to the relative sizes of the energy differences involved, the atom can be considered to be in an eigenstate of the total nuclear angular momentum $\hbar\vec{I}$. Except in cases of small fine-structure splitting, it is also

appropriate to consider the atom to be in an eigenstate of the total electronic angular momentum $\hbar\vec{J}$. In the absence of the hyperfine interaction, an atom possesses a $(2I+1)(2J+1)$-fold degeneracy. The effect of $\mathcal{H}_{\text{hyperfine}}$ is to reduce this degeneracy by splitting each of the eigenstates of $\mathcal{H}_{\text{electronic}}$ into $2X+1$ levels, X being the smaller of I or J. These $2X+1$ levels are characterized by the quantum number F, where

$$\vec{F} = \vec{I} + \vec{J} \tag{2-2}$$

and the total atomic angular momentum is $\hbar\vec{F}$. The $2X+1$ "F levels" are themselves $(2F+1)$-fold degenerate. Because $\mathcal{H}_{\text{atomic}}$ has eigenstates characterized by I and J which are here considered constants, only $\mathcal{H}_{\text{hyperfine}}$ need be considered in evaluating $\mathcal{H}_{\text{atomic}}$, thus:

$$\mathcal{H}_{\text{atomic}} = \mathcal{H}_{\text{hyperfine}} . \tag{2-3}$$

Schwartz (Schwartz, 1955) has shown that the hyperfine interaction energy may be written as a product of reduced nuclear and electronic multipole operators of order λ, and a Wigner 6 - j symbol appropriate to coupling of nuclear and electronic angular momenta through the multipole operators. The hyperfine energy E_F is given by:

$$E_F = \sum_{\lambda} E_F(\lambda) \qquad (\lambda = 1,2,3\ldots)$$

$$= \sum_{\lambda} (-)^{I+J-F} \begin{Bmatrix} F & J & I \\ \lambda & I & J \end{Bmatrix} \langle I \| Q_{\lambda}^{\text{nuc.}} \| I \rangle \langle J \| Q_{\lambda}^{\text{elect.}} \| J \rangle \tag{2-4}$$

where $Q_{\lambda}^{\text{nuc.}}$ and $Q_{\lambda}^{\text{elect.}}$ are nuclear and electronic multipole operators of order λ. The 6 - j symbol has the property that it vanishes unless the triads (I,I,λ), (J,J,λ) and (I,J,F) each add vectorially to form a triangle. For Na^{23} $J = 1/2$ and the only non-vanishing term in equation (2-4) is for $\lambda = 1$. Thus, in this case, only dipole interactions need be considered in

evaluating the hyperfine energy. This is a purely quantum mechanical result; classical electro-magnetic theory would predict the presence of all orders of multipole terms. Parity considerations show that electric dipole term vanishes and, therefore, only the magnetic dipole moment need be considered in evaluating E_F. It is convenient, for the case J or I = 1/2, to write the hyperfine energy as:

$$E_F = h\, a\, \vec{I} \cdot \vec{J} \qquad (2\text{-}5)$$

where a is the magnetic dipole interaction constant which is defined by:

$$h\, a = - \frac{\mu_I}{I} \frac{\vec{H}_J(0) \cdot \vec{J}}{J \cdot J} \qquad (2\text{-}6)$$

where μ_I is the nuclear dipole magnetic moment and $\vec{H}_J(0)$ is the magnetic field produced by the atom's electrons at the nucleus. In equation (2-6), it has been assumed that the nucleus is a point charge. This is not really correct and, in fact, the finite size of the nucleus gives rise to the hyperfine anomaly.

2. Atomic Hyperfine Structure in the Presence of an External Magnetic Field

In this section, the hyperfine structure of an atom in the presence of external magnetic fields will be considered.

If an atom is subject to a weak, uniform, static magnetic field, then the degeneracies remaining in $\mathcal{H}_{\text{hyperfine}}$ are completely removed (Zeeman effect). In this case, the atomic Hamiltonian is:

$$\mathcal{H}_0 = \mathcal{H}_{\text{hyperfine}} + \mathcal{H}_{\text{magnetic}} \qquad (2\text{-}7)$$

Traditionally, in ABMR parlance, the magnet which produces this weak, static field is called the "C magnet" and its field will be denoted as $\vec{H}_c$. The

direction of $\vec{H}_c$ is taken to define the Z axis. $\mathcal{H}_{\text{magnetic}}$ is given by:

$$\mathcal{H}_{\text{magnetic}} = (-g_J \mu_0 m_J - g_I \mu_0 m_I) \; H_c \qquad (2\text{-}8)$$

where $g_J = \frac{\mu_J}{J \mu_0}$, $g_I = \frac{\mu_I}{I \mu_0}$, μ_0 is the Bohr magneton, both μ_J and μ_I are in Bohr magnetons. Since $\vec{H}_c$ destroys spherical symmetry, F is not a good quantum number. In weak fields, however, it is nearly so and, in any case, it is useful to keep track from which F level a particular magnetic substate adiabatically develops. Thus, these levels are denoted as $|(F),m_F\rangle$ with the understanding that $\lim_{H_c \to 0} |(F),m_F\rangle = |F,m_F\rangle$. The terms $\mathcal{H}_{\text{magnetic}}$ and $\mathcal{H}_{\text{hyperfine}}$ are diagonal in the $|I,J,m_I,m_J\rangle$ and $|I,J,F,m_F\rangle$ representations respectively. Depending on their relative sizes, it is convenient to utilize the representation for which the off-diagonal elements are smallest. For the cases I or J = 1/2, thus limiting the number of F values to two, the secular determinant can be solved exactly. Such a solution is due to Breit and Rabi (Breit and Rabi, 1931). For $u_I > 0$ and $F = I \pm 1/2$, the result is

$$E_{F,m_F} = \frac{-h\Delta\nu}{2(2I+1)} - \frac{\mu_I}{I} H_c m_F \pm \left(\frac{h\Delta\nu}{2}\right) 1 + \frac{4m_F x}{2I+1} + x^2 \Big)^{1/2} \qquad (2\text{-}9)$$

where $x = -\dfrac{\frac{\mu_J}{J} + \frac{\mu_I}{I}}{h\Delta\nu} H_c$. The plus sign denotes the upper F state and minus sign denotes the lower F state. The term $h\Delta\nu$ is the energy difference between the two F states at zero magnetic field and is called the "hyperfine splitting". Figure 1 is a plot of E_{F,m_F} as a function of x for Na^{23}. It can be seen that as x increases, the levels of each multiplet deviate increasingly from equal spacing. The MQT discussed in this

Figure 1

Breit-Rabi Diagram for Na^{23}

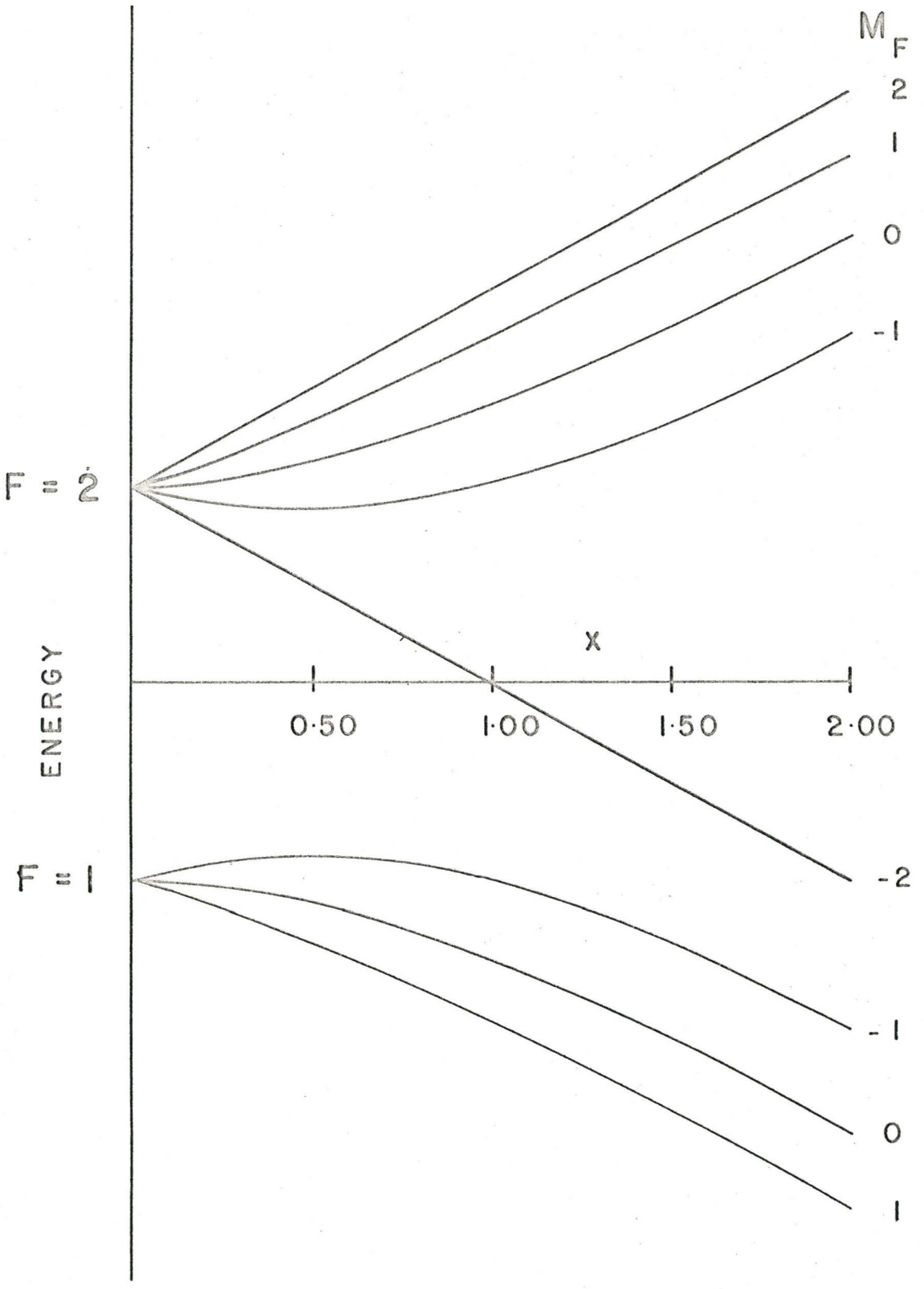
M F
2
1
0
-1
F = 2
ENERGY
X
0·50
1·00
1·50
2·00
F = 1
-2
-1
0
1

work takes place between the magnetic sub-levels of a given multiplet, i.e. they obey the selection rule, $\Delta F = 0$, $\Delta m_F = \pm n$. Thus, for $x > 0$, the different order of MQT occurs at distinct resonance frequencies in accordance with equation (1-2), $|E_f - E_i| = n\hbar\omega$. This makes it experimentally possible to isolate the different MQT so that the behaviour of one can be studied without significant contribution to its transition probability from the other MQT.

Figure 2 is a plot of the nominal frequency differencies between the 1-quantum transition and the MQT. The plot is presented as a function of the static field parameter x. The frequency ν_n of an n-quantum transition is

$$\nu_n = \frac{|E_f - E_i|}{nh} .$$

Figure 2

Nominal Resonance Frequencies

The 1-quantum resonance frequency, ν_{1Q}, is given by the dashed line. The n-quantum resonance frequencies are found by subtracting the appropriate frequency difference from ν_{1Q}.

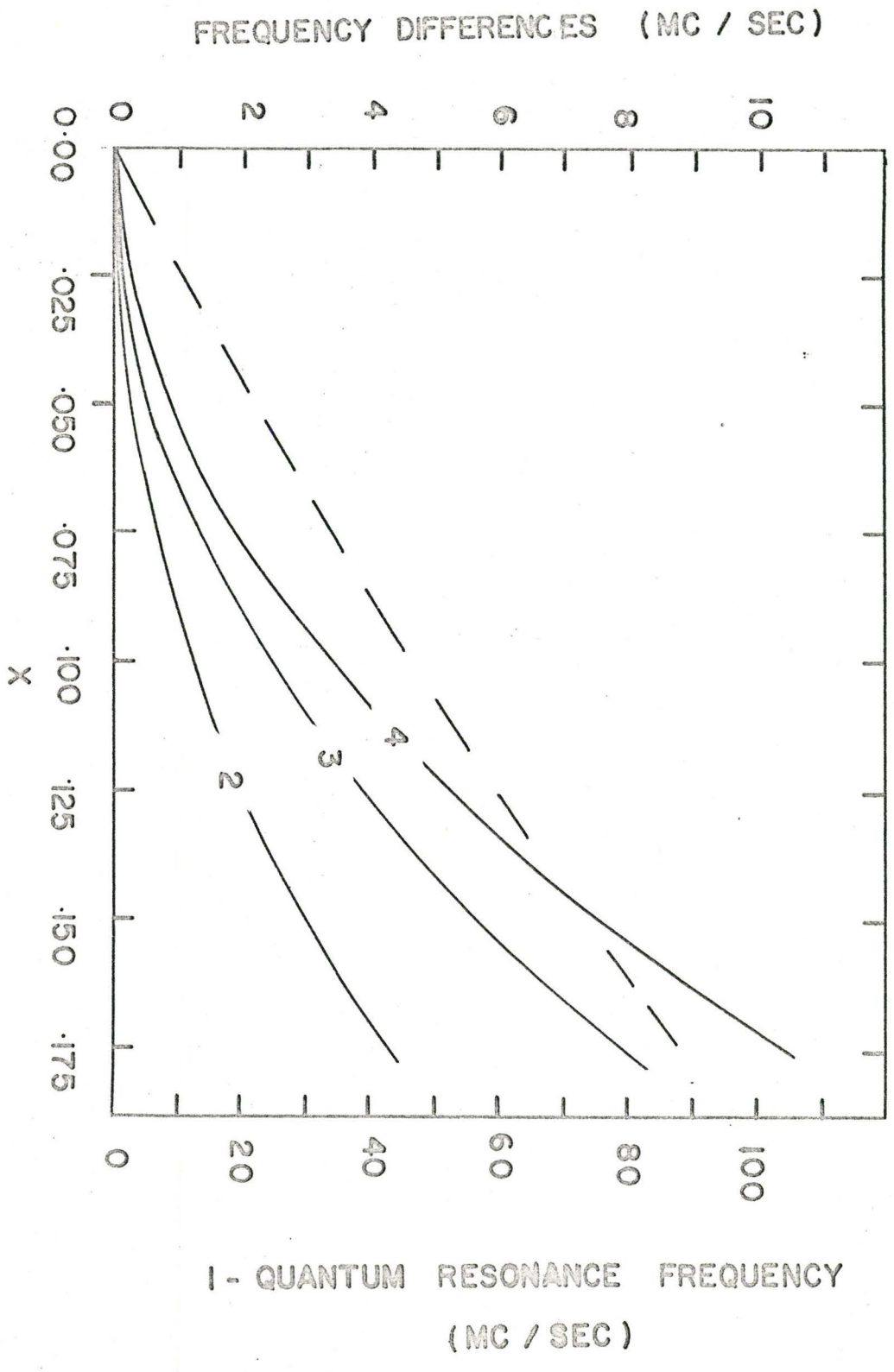
FREQUENCY DIFFERENCES (MC / SEC)
0
2
4
6
8
10
0·00
·025
·050
·075
·100
·125
·150
·175
X
2
3
4
0
20
40
60
80
100
1 - QUANTUM RESONANCE FREQUENCY
(MC / SEC)

CHAPTER III

INDUCED TRANSITIONS

1. Development of the Interaction Matrix

In this chapter, expressions for the transition probability of MQT between the magnetic substates of an atomic hyperfine multiplet are developed. The transitions are assumed to have been induced by an oscillating magnetic field. The direction of the oscillation field is taken as being perpendicular to the Z axis, along an axis which can be defined as the X axis. Transitions induced by such a field are known as "π transitions". The oscillating field, $\vec{H}_{rf}$, is given by

$$\vec{H}_{rf} = (H_o \cos(\omega t))\hat{X} = \frac{H_o}{2}(e^{i\omega t} + e^{-i\omega t})\hat{X} \qquad (3\text{-}1)$$

where H_o is the oscillating field's amplitude and $\hat{X}$ is a unit vector in the x direction. This definition of $\vec{H}_{rf}$ assumes that atoms travel through a region of uniform field amplitude.

In the presence of the oscillating field $\vec{H}_{rf}$ and the static field $\vec{H}_c$, the atomic Hamiltonian is

$$\mathcal{H} = \mathcal{H}_o + V(t) \qquad (3\text{-}2)$$

where $\mathcal{H}_o = \mathcal{H}_{hyperfine} + \mathcal{H}_{magnetic}$ and V(t) is a time-dependent perturbation due to the applied oscillating field $\vec{H}_{rf}$. It is now necessary to find the matrix elements of V(t). For an atom possessing a magnetic dipole $\vec{\mu} = \mu_o(g_J\vec{J} + g_I\vec{I})$, the interaction energy due to the presence of $\vec{H}_{rf}$ is

$$\mathcal{H}_{rf} = -\vec{\mu}\cdot\vec{H}_{rf} = -1/4\,\mu_o H_o\left\{(g_J - g_I)(J_+ + J_-) + g_I(F_+ + F_-)\right\}(e^{i\omega t} + e^{-i\omega t}), \qquad (3\text{-}3)$$

The x components of $\vec{I}$ and $\vec{J}$ have been expressed in the standard representation of the angular momentum raising and lowering operators $J_{\pm}$ and $F_{\pm}$ (e.g. Messiah, 1962). Thus $\mathcal{H}_{rf}$ only connects states that differ by one unit of angular momentum.

In the limit of vanishing static fields, $H_c \rightarrow 0$, F is a good quantum number and the matrix elements $\langle F', m_F' | \mathcal{H}_{rf} | F, m_F \rangle$ can be expressed as functions of I, J, F', F, m_F and m_F' through the use of equation (3-3). Following Salwen (Salwen, 1956), a parameter b is defined as

$$\hbar b = \frac{\mu_o H_o (g_I - g_J)}{4(2I + 1)} \propto H_o \quad . \tag{3-4}$$

Thus

$$\langle F', m_F' | \mathcal{H}_{rf} | F, m_F \rangle = \hbar b (e^{i\omega t} + e^{-i\omega t}) \langle F', m_F' | \left\{ (2I+1)(J_+ + J_-) + \frac{(2I+1) g_I}{g_J - g_I} (F_+ + F_-) \right\} | F, m_F \rangle . \tag{3-5}$$

Using expressions for $(J_+ + J_-) | F, m_F \rangle$ and $(F_+ + F_-) | F, m_F \rangle$, see Condon and Shortley, 1936, the matrix elements of $\mathcal{H}_{rf}$ can be found. Equation (3-5) is written in terms of a matrix element $\tilde{\alpha}(F', m_F'; F, m_F)$ as

$$\langle F', m_F' | \mathcal{H}_{rf} | F, m_F \rangle = \hbar b (e^{i\omega t} + e^{-i\omega t}) \tilde{\alpha} (F', m_F'; F, m_F) . \tag{3-6}$$

so that the angular momentum dependence of $\mathcal{H}_{rf}$ is in the terms $\tilde{\alpha} (F', m_F'; F, m_F)$. For the case $J = 1/2$, $F = I + 1/2$, $\Delta F = 0$, i.e. transitions between the magnetic sublevels of a given state, the $\tilde{\alpha}(F', m_F'; F, m_F)$ are given by

$$\tilde{\alpha} (I + 1/2, m_{F-1}; I+1/2; m_F) = \left[(I + 1/2 + m_F)(I + 3/2 - m_F) \right]^{1/2} \left\{ 1 + \frac{(2I + 1) g_I}{g_J - g_I} \right\} . \tag{3-7}$$

Neglecting the small term in g_I, Equation (3-7) yields

$$\begin{aligned} \tilde{\alpha}(2,2;2,1) &= 2 \\ \tilde{\alpha}(2,1;2,0) &= 6 \\ \tilde{\alpha}(2,0;2,-1) &= 6 \\ \tilde{\alpha}(2,-1;2,-2) &= 2 . \end{aligned} \tag{3-8}$$

When the static field H_c is non-zero, F is no longer a good quantum number. Because the terms $\tilde{\alpha}(F',m_F';F,m_F)$ hold only for states of specified values of F (i.e. only when F is a good quantum number), the states $|(F),m_F\rangle$ appropriate to non-zero values of H_c must be expressed in terms of states of specified F, $|F,m_F\rangle$; i.e. $|(F),m_F\rangle$ is expanded using the states $|F,m_F\rangle$ as basis vectors. Thus:

$$|(F),m_F\rangle = \sum_{F'} a_{F'} |F',m_F'\rangle \tag{3-9}$$

where F' is taken over all possible F's resulting from the coupling of I and J. The convention is now adopted that $\tilde{\alpha}(F',m_F';F,m_F)$ is written with the tilda only for the case $H_c = 0$, and the tilda will be removed from $\tilde{\alpha}(F',m_F';F,m_F)$ when $H_c \neq 0$. For $\Delta F = 0$ transitions, the label F may be dropped from $\alpha(F,m_F';F,m_F)$ as may the subscripts F on the m_F, thus

$$\alpha(F,m_F';F,m_F) \longrightarrow \alpha_{m,m'} \tag{3-10}$$

Then, for $\Delta F = 0$ transitions, $\mathcal{H}_{r.f.}$ can be written as $\mathcal{H}_{r.f.} =$

$$\begin{pmatrix} 0 & \hbar b \alpha_{-F,-F+1} (e^{i\omega t} + e^{-i\omega t}) & 0 & \cdots \\ \hbar b \alpha_{-F+1,-F} (e^{i\omega t} + e^{-i\omega t}) & 0 & \hbar b \alpha_{-F+1,-F+2} (e^{i\omega t} + e^{-i\omega t}) & \cdots \\ 0 & \hbar b \alpha_{-F+2,-F+1} (e^{i\omega t} + e^{-i\omega t}) & 0 & \cdots \\ \cdot & \cdot & \cdot & \cdot \\ \cdot & \cdot & \cdot & \cdot \\ \cdot & \cdot & \cdot & \cdot \end{pmatrix} \tag{3-11}$$

The eigenenergies of $\mathcal{H}_o = \mathcal{H}_{hyperfine} + \mathcal{H}_{magnetic}$ satisfy

$$\mathcal{H}_o \Psi_m = \hbar \omega_{(m)} \Psi_m \qquad (3\text{-}12)$$

where the convention adapted is that $\omega_{(m)} < \omega_{(m+1)}$, corresponding to the assumption of a positive nuclear magnetic moment.

The matrix element of the i^{th} row and j^{th} column of the matrix $\mathcal{H}_{r.f.}$, equation (3-11), is denoted as $\mathcal{H}_{r.f.}(i,j)$. The off-diagonal matrix elements $\mathcal{H}_{r.f.}(j,j+1)$ represent transitions to states of lower energy. These matrix elements are written with the negative exponent only, the positive exponent having been dropped. Similarly, the off-diagonal matrix elements $\mathcal{H}_{r.f.}(j+1,j)$ which represent an increase in the system's energy are written with only the positive exponent retained.* The counter rotating components have been dropped because otherwise it is impossible to obtain certain analytic expressions required in the formulation of MQT probabilities.

Applying these arguments, $V(t)\Psi_m$ is given by

$$V(t)\Psi_m = h b \left[\alpha_{m,m+1} \Psi_{m+1} e^{-i\omega t} + \alpha_{m,m-1} \Psi_{m-1} e^{+i\omega t} \right] \qquad (3\text{-}13)$$

Equation (3-13) can be inserted into equation (3-3) yielding $\mathcal{H}(t) = \mathcal{H}_o + V(t)$. This expression, in conjunction with equation (3-13), is now used to solve the problem of induced transition probabilities between the Zeeman levels of an atomic hyperfine multiplet, subject to the conditions

---

* Bloch and Siegert (Bloch and Siegert, 1940) have shown for the two-level system that the counter rotating component contributes a term to the probability expression $\sigma \frac{1}{\omega + \omega_o}$, where $\omega_o = \frac{E_f - E_i}{h}$ which is small compared to the so-called resonance denominator term $\frac{1}{\omega_o - \omega}$ for $\omega \simeq \omega_o$.

that all atoms experience, the perturbation V(t) for a time t, and that the r.f. field is of uniform amplitude H_o over its extent.

2. Two-Level Case

Although the case of two-levels can be derived in more direct ways, (Ramsey, 1956), it is convenient here to use the formulation developed above and set $J = \frac{1}{2}$, $I = 0$. Thus, $F = \frac{1}{2}$ and $m_F = \pm \frac{1}{2}$. For this case $\alpha_{\frac{1}{2},-\frac{1}{2}} = \alpha_{-\frac{1}{2},\frac{1}{2}} = 1$. Hence $\mathcal{H}$ is

$$\mathcal{H} = \begin{pmatrix} W_{-\frac{1}{2}} & \hbar b\, e^{-i\omega t} \\ \hbar b\, e^{i\omega t} & W_{+\frac{1}{2}} \end{pmatrix} \tag{3-14}$$

The states $\left|\, (\tfrac{1}{2}),\ +\tfrac{1}{2} \right\rangle$ and $\left|\, (\tfrac{1}{2}),\ -\tfrac{1}{2} \right\rangle$ will be denoted as $|+\rangle$ and $|-\rangle$ respectively. Note that since there is only one F state for $I = 0$, $J = \frac{1}{2}$, then $\left|\, (\tfrac{1}{2})\ \pm \right\rangle \equiv \left|\, \tfrac{1}{2},\ \pm \right\rangle$. In terms of $|+\rangle$ and $|-\rangle$, the wave equation at a time t after the perturbation V(t) has been "switched on" is given by

$$\Psi(t) = A(t)|-\rangle + B(t)|+\rangle \tag{3-15}$$

Since $i\hbar \frac{\partial \Psi}{\partial t} = \mathcal{H}\Psi$, it follows that

$$\begin{aligned} A(t) &= -\frac{i}{\hbar} W_{-\frac{1}{2}} A(t) + \hbar b\, e^{-i\omega t} B(t) \\ B(t) &= -\frac{i}{\hbar} W_{+\frac{1}{2}} B(t) + \hbar b\, e^{+i\omega t} A(t) \end{aligned} \tag{3-16}$$

If it is assumed that at $t = 0$, the system is in $|-\rangle$ then $A(0) = 1$, $B(0) = 0$. These initial conditions permit solutions to equation (3-16) which are

$$\begin{aligned} A(t) &= (i \cos\theta \sin \tfrac{1}{2}at + \cos \tfrac{1}{2}at)\, e^{\,i(\frac{1}{2}\omega - (W_{\frac{1}{2}} + W_{-\frac{1}{2}})/2\hbar)\, t} \\ B(t) &= i \sin\theta \sin \tfrac{1}{2}\omega t\, e^{\,i\left(-\frac{1}{2}\omega - (W_{\frac{1}{2}} + W_{-\frac{1}{2}})/2\hbar\right)\, t} \end{aligned} \tag{3-17}$$

where

$$\cos\theta = (\omega_o - \omega)/a$$

$$\sin\theta = -2b/a$$

$$a = (\omega_o - \omega)^2 + (2b)^2 \quad \text{and}$$

$$\omega_o = (W_{\frac{1}{2}} - W_{-\frac{1}{2}})/\hbar \ .$$

Thus the probability that a transition from state $|-\rangle$ to a state $|+\rangle$ in the time $t = \tau$ is (Rabi, 1937):

$$P_{-\frac{1}{2},\frac{1}{2}} = \frac{(2b)^2}{(\omega_o - \omega)^2 + (2b)^2} \sin^2\left(\tfrac{1}{2}\left[(\omega_o - \omega)^2 + 2b^2\right]^{\frac{1}{2}} \tau\right) \qquad (3\text{-}18)$$

where ω is the angular frequency of the oscillating field.

Figure 3 is a plot of $P_{-\frac{1}{2},\frac{1}{2}}$ as a function of $\frac{|\omega_o - \omega|}{2\pi}$ for two choices of b. That value of b for which $P_{-\frac{1}{2},\frac{1}{2}}$ equals unity at $\omega = \omega_o$ is called "optimum b" and will be denoted as "b_{opt}".

3. More Than Two-Levels, Equally Spaced in Energy

Majorana (Majorana, 1932) was the first to obtain transition probabilities for systems having more than two levels. His formula may be derived by synthesizing a general spin $\hbar\vec{F}$ and wave function $|F,m_F\rangle$ from a sum of 2F Pauli spin matrices and the product of the wave function for the k^{th} angular momentum of spin $\frac{1}{2}$ parallel to the Z axis respectively. Thus

$$F = \sum_{k=1}^{2F} \tfrac{1}{2}\sigma_k$$

$$|F,m_F\rangle = \sum_{k=1} \tfrac{1}{2}\eta_k \qquad (3\text{-}19)$$

Figure 3

Two-Level Resonance Line Shape

The solid curve corresponds to $b = b_{opt} = 0.06$ Mc/sec. The dashed curve is for $b = 0.09$ Mc/sec. The subsidiary maxima are attributed to the calculated transition probability not having been velocity averaged. For this calculation, τ is 4 microseconds.

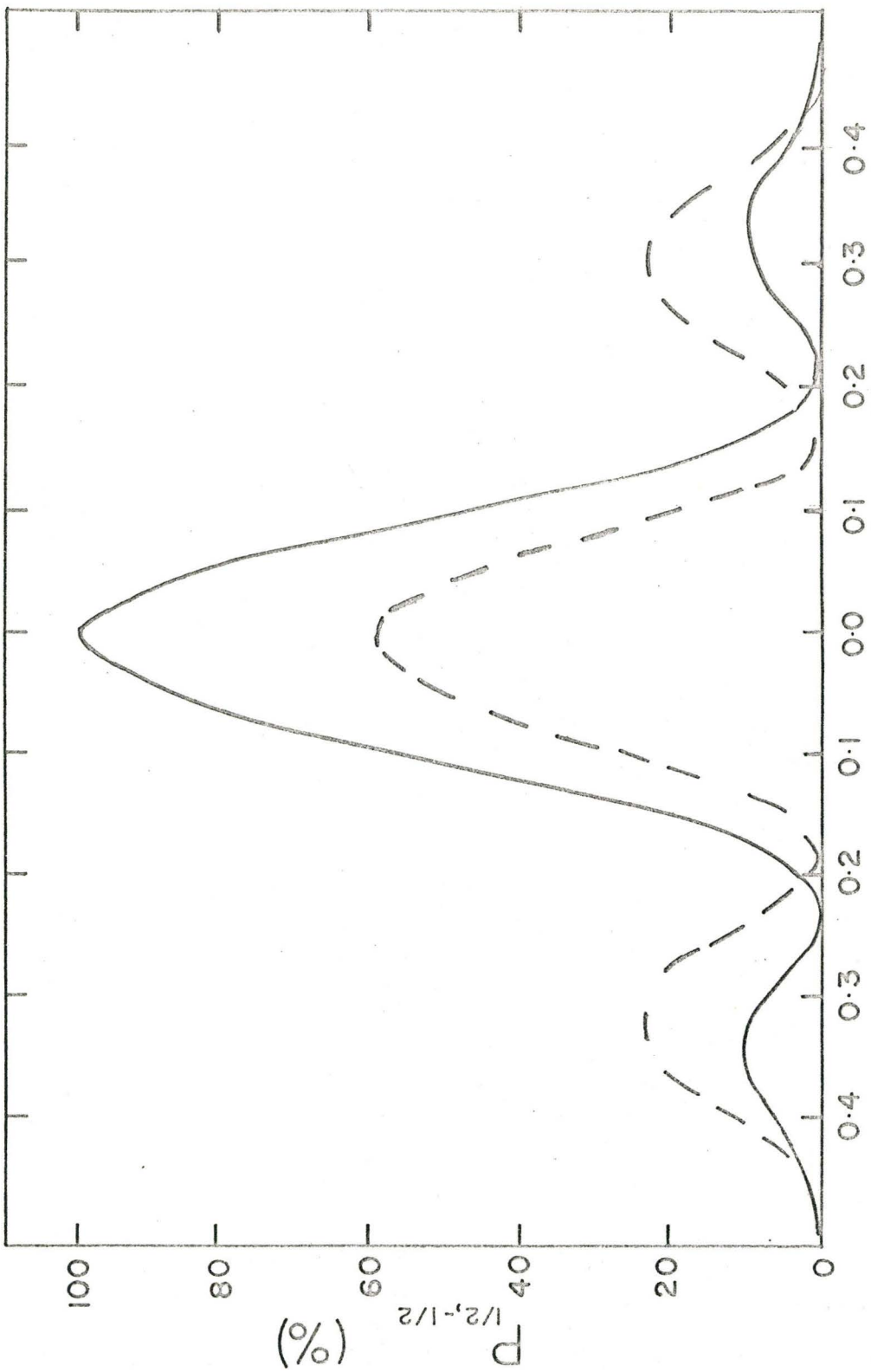
100
80
60
40
20
0
$P_{1/2,-1/2}$ (%)
0·4
0·3
0·2
0·1
0·0
0·1
0·2
0·3
0·4
$|\nu - \nu_0|$ (MC/SEC)

where Γ_k and Υ_k are the k^{th} spinor and wave functions of the angular momentum respectively. Majorana's derivation assumes that all the magnetic sublevels are equally spaced and that $\vec{H}_{r.f.}$ acts in the same way upon each level. After $\vec{H}_{r.f.}$ has been applied for a time t, the wave function is

$$\Psi(t) = \sum_{m'} C_{mm'}(t) \mid F, m_F \rangle \qquad (3\text{-}20)$$

where $C_{m,m'}(t) = G(F,m,m') \langle m \mid V(t) \mid m' \rangle$

and $G(F,m,m')$ is a factor due to normalization constants appearing in the angular momentum raising and lowering operators. Now $\langle m \mid V(t) \mid m' \rangle = \hbar b (e^{\pm i\omega t}) \times \alpha_{m,m'}$, but, since it is assumed that V(t) acts the same way on all m levels, $\alpha_{m,m'}$ is chosen to be equal to unity. Thus, $\langle m \mid V(t) \mid m \rangle$ is identical to the perturbation V(t) for the two-level case described above.

The probability of the transition $m \leftrightarrows m'$ is $\mid C_{m,m'} \mid^2$. This yields

$$P_{m,m'} = (F-m)!\,(F+m)!\,(F-m')!\,(F+m')!\,(\sin \tfrac{1}{2}\theta)^{4F} \times \left\{ \sum_r \frac{(-)^r\,(\cot \tfrac{1}{2}\theta)^{m+m'+2r}}{(F-m-r)!\,(F-m'-r)!\,(m+m'+r)!\,r!} \right\}^2 \qquad (3\text{-}21)$$

where r = 0, 1, 2, ... r max, r max being the largest value of r for which none of the arguments of the factorials is negative. Also, $\sin^2 \tfrac{1}{2}\theta = P_{-\frac{1}{2},\frac{1}{2}}$ as in equation (3-18), i.e. it is the transition probability appropriate to the two-level case.

Figures 4a and 4b are plots of $P_{m,-2}$ (m = -1,0,1,2) at the nominal resonance frequency $\omega = \omega_o$, as a function of b. Below their intensity

Figures 4a and 4b

Power Dependence of MQT at Resonance Frequency Using the Majorana Formula

The time, τ, is 4 microseconds.

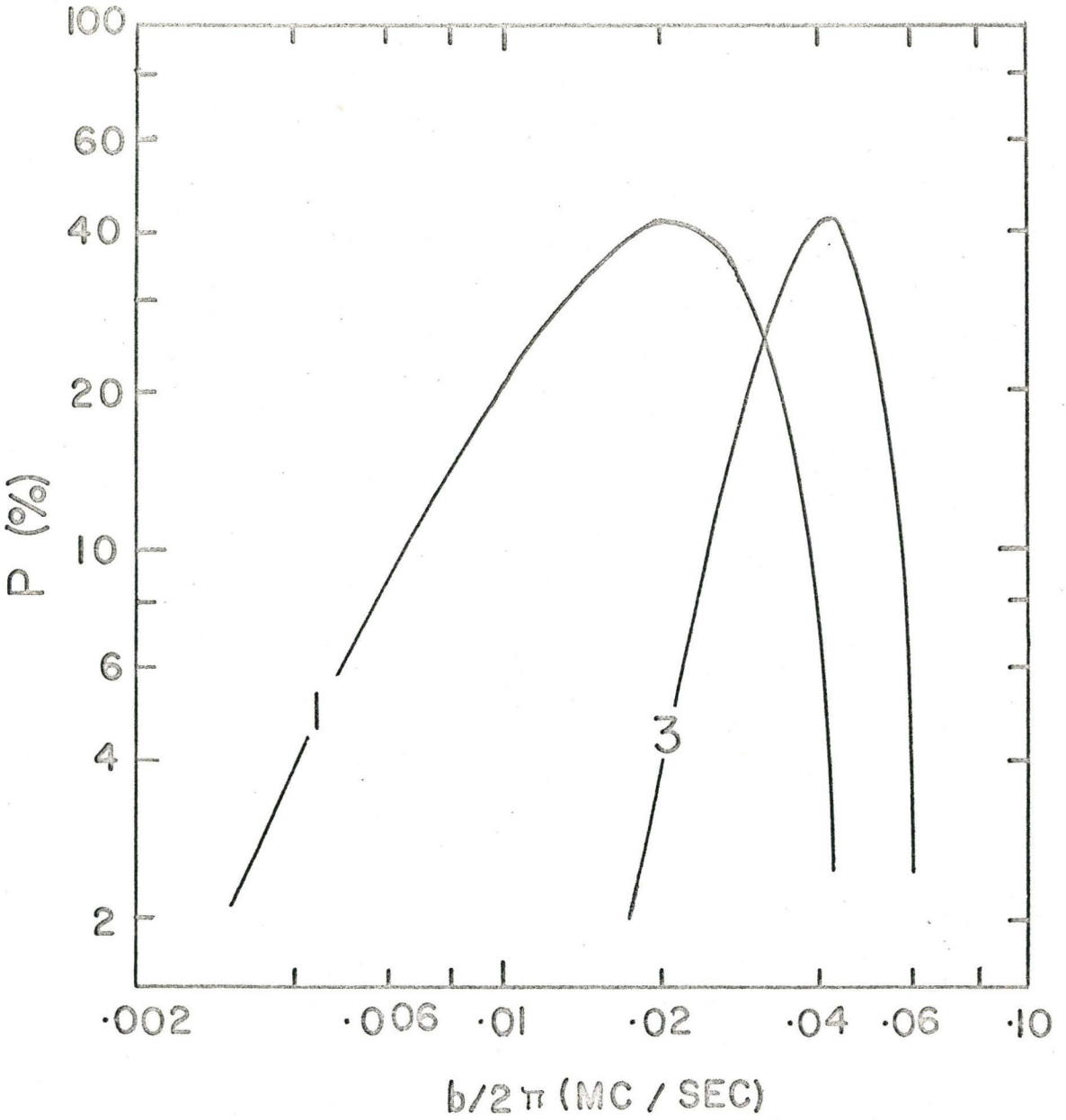
100
60
40
20
10
6
4
2
P (%)
1
3
·002
·006
·01
·02
·04
·06
·10
b/2π (MC / SEC)

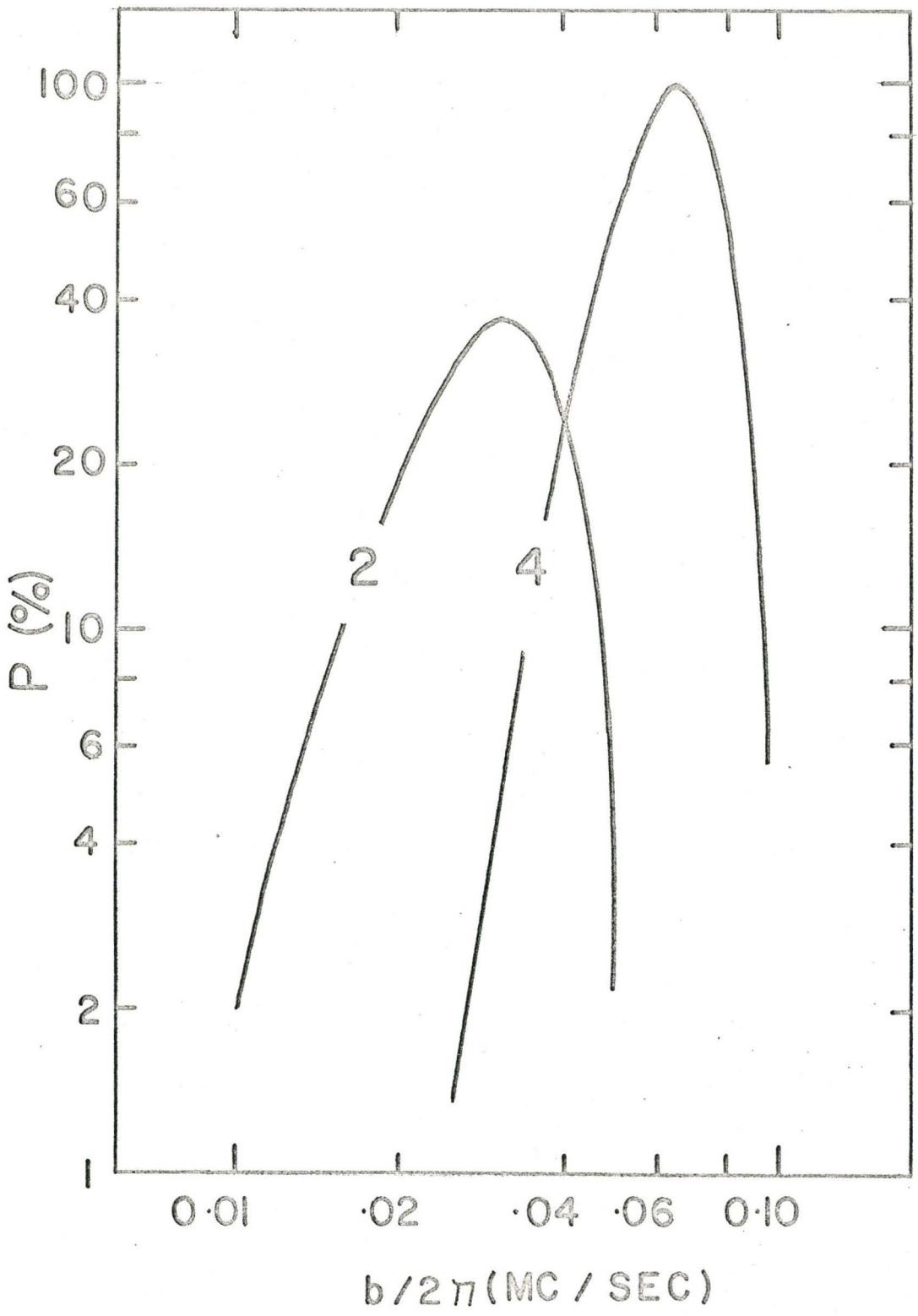
100
60
40
20
10
6
4
2
1
P (%)
2
4
0·01
·02
·04
·06
0·10
b/2π (MC / SEC)

peaks, these curves exhibit clearly straight portions, the slopes of which appear to be determined by transition multiplicity. This observation motivated the "power dependence" experiments performed in this work. The value of b corresponding to the maxima of $P_{m,-2}$ are the values of b_{opt} appropriate to the transition involved.

4. More Than Two-Levels, Quite Unequally Spaced

Perturbation methods have been used by several authors to obtain multiple quantum transition probabilities when the levels are unequally spaced. Discussion in this work will be limited to the theories of Salwen (Salwen, 1955) and Hack (Hack, 1956).

H. Salwen utilizes a transformation to a rotating co-ordinate system (see Rabi et al., 1954) to obtain the interaction matrix. The co-ordinate system rotates at an angular frequency ω about the Z axis, so that one component of the oscillating field $\vec{H}_{r.f.} = \frac{H_o}{2} \hat{x} (e^{i\omega t} + e^{-i\omega t})$ appears static to an observer in the rotating frame. The other component can be neglected for reasons given above. Such a picture leads to the time independent Hamiltonian

$$\mathcal{H}' = \mathcal{H}_o - m\omega + \frac{\mu_o}{h} \frac{H_o}{2} (g_1 (V_1)_x + \ldots g_b (V_b)_x) \qquad (3\text{-}22)$$

where $(V_b)_x$ is the x component of the b^{th} value of $\vec{V}$. The symbol $\vec{V}$ stands for any angular momentum vector, here, the two values of $\vec{V}$ are $\vec{I}$ and $\vec{J}$. Because the MQT obey the selection rules $\Delta F = 0$, $\Delta m_F = \pm n$, the states $|(F), m_F\rangle$ will be denoted as $|m\rangle$. In this representation, the rotating field will connect two levels $|m\rangle$ and $|m'\rangle$ if they are degenerate in the rotating frame, or, equivalently, if $\mathcal{H}'|m\rangle = \mathcal{H}'|m'\rangle$. For non-zero

values of H_c, the levels $|m\rangle$ and $|m'\rangle$ are not degenerate in the space fixed frame, or $\mathcal{H}_o|m\rangle \neq \mathcal{H}|m'\rangle$. Because of the assumption appropriate to this subsection, namely that the levels are quite unequally spaced, it follows that the different MQT resonance frequencies are isolated from one another, as was demonstrated in Chapter II. For frequencies in the neighbourhood of $\omega = \frac{|E_f - E_i|}{n\hbar}$ ' has only two, and no more, degenerate eigenstates. Thus, if the initial state is $|m\rangle$ and the final state is $|m'\rangle$, then for frequencies in the region $\omega = \frac{|E_m - E_{m'}|}{|m - m'|\,\hbar}$ only the states $|m\rangle$ and $|m'\rangle$ will be strongly mixed -- all the other $2F+1$ substates of F will remain unmixed. Then $\mathcal{H}'$ may be approximated by a two-dimensional matrix $\mathcal{H}''$, containing terms appropriate to the two states $|m\rangle$ and $|m'\rangle$. Salwen develops the matrix elements of $\mathcal{H}''$ by considering the expansion of the ket $|\ \rangle$ as a linear combination of the (nearly) degenerate states $|m\rangle$ and $|m'\rangle$:

$$|\ \rangle = |m\rangle\langle\ |\ \rangle + |m'\rangle\langle m'|\ \rangle + \sum_{n \neq m,m'} |n\rangle\langle n|\ \rangle. \qquad (3\text{-}23)$$

This enables Salwen to solve the matrix equation

$$\mathcal{H}'' \begin{pmatrix} \langle m|\ \rangle \\ \langle m'|\ \rangle \end{pmatrix} = E \begin{pmatrix} \langle m|\ \rangle \\ \langle m'|\ \rangle \end{pmatrix} \qquad (3\text{-}24)$$

The degenerate eigenvalues of $\mathcal{H}''$ are used (with the proper root selected) to calculate the eigenvector $\begin{pmatrix} \langle m|\ \rangle \\ \langle m'|\ \rangle \end{pmatrix}$. By reinserting derived values into equation (3-24), the eigenvectors may be found, in principle, to any desired degree of accuracy.

Using terms to the lowest order in r.f. amplitude that give non-vanishing probabilities for a given transition, Salwen obtains

$$P_{m,m'} \simeq \frac{b^2_{m,m'}}{(\omega^*_{m,m'} + \omega)^2 + b^2_{m,m'}} \left(\sin^2 \left(n\pi \sqrt{(\omega^*_{m,m'} - \omega)^2 + b^2_{m,m'}}\ \tau \right) \right) \qquad (3\text{-}25)$$

where $\omega^*_{m,m'}$ is the n-quantum resonance frequency, and is given by

$$\omega^* = \omega_{m,m'} \mp \left(\frac{b^2}{n}\right) \left\{ \sum_{i=m-1} \frac{|\alpha_{i,m}|^2}{\omega_{m,i} - \omega_{m,m'}} + \sum_{i=m+1} \frac{|\alpha_{i,m}|^2}{\omega_{m,m'} - \omega_{m,i}} \right.$$

$$\left. - \sum_{i=m'-1} \frac{|\alpha_{i,m'}|^2}{\omega_{m',i} - \omega_{m,m'}} - \sum_{i=m'+1} \frac{|\alpha_{i,m'}|^2}{\omega_{m,m'} - \omega_{m',i}} \right\} + \mathcal{O}(b^4). \qquad (3\text{-}26)$$

where $\omega_{m,m'} = \dfrac{E_m - E_{m'}}{n\,h}$ is the nominal n-quantum resonance frequency and the states i are the states intermediate to m and m'. The term $b_{m,m'}$ is given by

$$b_{m,m'} = 2b\,\alpha_{m,m'} + \mathcal{O}(b^2) \qquad m = m' \pm 1$$

$$b_{m,m'} = \frac{2}{n} b^n \sum_{\substack{i=m\pm1 \\ i'=m\pm2 \\ \vdots \\ i^{(n-1)} = m\pm(n-1)}} \frac{\alpha_{m,i}\ \alpha_{i',i''} \cdots \alpha_{i(n-1),m'}}{(\nu_{m,m'} - \nu_{m',i})(\nu_{m,m'} - \nu_{m',i'}) \cdots (\nu_{m,m'} - \nu_{n,i(n-1)})} \qquad (3\text{-}27)$$

$+ \mathcal{O}(b^{n+2})$ for $n \geq 2$, where $\nu_{m,m'} = \dfrac{\omega_{m,m'}}{2\pi}$.

Along the way to equation (3-25), Salwen has assumed that in the vicinity of $\omega^*_{m,m'}$, changes, with respect to ω, of the off-diagonal matrix elements and parts of the diagonal matrix elements of $\mathcal{H}''$ can be ignored. This approximation, together with the assumption that only two of the eigenstates of $\mathcal{H}'$ are degenerate for $\omega \simeq \omega^*_{m,m}$, limit the solution to the case of quite unequally spaced levels. Two normalization factors, appearing as a

product, have been taken so that the product equals unity. Use was also made of expressions which related MQT probabilities to the general eigenstates $|\lambda\rangle$ in the rotating co-ordinate system for the case that the rotating field is applied for a time τ.

Equation (3-25) is of the form of the single quantum transition probability (equation (3-18)) except that γ in equation (3-18) has been replaced by $n\gamma$ for the n-quantum transition. In an ABMR experiment, there is a resonance broadening in accord with the uncertainty principle

$$\Delta\upsilon \simeq \frac{1}{\tau} \qquad (3\text{-}28)$$

where τ is the length of time the atom is subject to the transition inducing oscillating field. Since, by equation (3-25), for an n-quantum transition γ (single quantum) appears to be a factor of n greater, it is to be expected that the full width at half maximum (FWHM) of an n-quantum resonance will be n times more narrow than a one-quantum line shape, all other factors being equal. At resonance frequency and small r.f. amplitude $P_{m,m'} \simeq \sin(n\pi H_o^n \tau) \propto H_o^{2n}$. Thus, greater r.f. amplitudes are required to give equal transition probabilities as multiplicity increases. From equation (3-26), $\omega^* \simeq \omega_{m,m'} \pm O(b^2)$, thus resonances are expected to shift as the square of r.f. amplitude away from the nominal n-quantum resonance frequency $\omega_{m,m'} = \frac{|E_m - E_{m'}|}{|m - m'|\hbar}$.

These results qualitatively describe the known behaviour of MQT. They do exhibit progressively more narrow FWHM as n increases; they do exhibit increased intensity sensitivity to changes in r.f. field amplitude as multiplicity increases and do require greater amplitudes for comparable intensities as multiplicity increases.

For the special case that the levels are exactly equally spaced (normal Zeeman effect), Salwen obtains an exact solution which is identical to that of Majorana.

M. Hack (Hack, 1956) uses the methods of time-dependent perturbation theory to obtain MQT probability expressions. Terms are obtained to the lowest order for which a non-vanishing transition probability occurs for the transition under consideration. Of course, the use of lowest order perturbation theory limits the results to the case of small amplitudes of oscillating field. It is also assumed that the various MQT resonance frequencies are well separated.

The eigenstates of $\mathcal{H}_o = \mathcal{H}_{hyperfine} + \mathcal{H}_{magnetic}$ are evolved according to the well known time-dependent relation valid to any order n

$$\Psi_j(t) = \sum_i a_{ij}(t)\, e^{-i\hbar\omega_i t/\hbar}\, \Psi_i \qquad (3\text{-}29)$$

where $\hbar\omega_i$ are the eigenenergies satisfying $\mathcal{H}_o \Psi_i = \hbar\omega_i \Psi_i$. The coefficients $a_{ij}(t)$ are given by

$$a_{ij}^{(n)}(t) = -\frac{i}{\hbar}\int_o^t \sum_\ell \Theta_{i\ell}\, e^{-i\omega_{i\ell}t'}\, a_{\ell j}^{(n-1)}(t)\quad dt' \qquad (3\text{-}30)$$

where $\Theta_{i\ell}$ is a time independent matrix corresponding to the time-dependent perturbation V(t), the time-dependence having been removed by transformation to a rotating co-ordinate system, and $\omega_{i\ell} = \omega_i - \omega_\ell$.

Using diagrams to assist in picking out the appropriate terms and their signs, Hack finds the n^{th} order coefficient $a_{ij}^{(n)}(t)$ to be

$$a_{ij}^{(n)}(t) = (-) \sum_{\ell,m,\ldots r} \frac{A_{i\ell} A_{\ell,m} \cdots A_{rj} \left\{ e^{i(\omega_{ij} \mp (n\omega)t} - 1 \right\}}{(\omega_{ij} \mp n\omega)(\omega_{\ell j} \mp (n-1)\omega) \ldots (\omega_{rj} \mp \omega)} \qquad (3\text{-}31)$$

Following his prescription, the next contribution is

$$+ (-)^{n-1} \sum_{\ell, m, \ldots q} \frac{A_{i\ell} A_{\ell m} \cdots A_{rq} \left\{ e^{i(\omega_{ij} \mp (n-1)\omega) t} - 1 \right\}}{(\omega_{ir} \mp (n-1)\omega)(\omega_{\ell r} \mp (n-2)\omega) \cdots (\omega_{qj} \mp \omega)}$$

where the initial state is denoted i, the final state j, and all the states intermediate to i and j are denoted by ℓ, m, n ... q, the matrix elements $A_{m\,n}$ satisfy $A_{m\,n} \equiv \hbar\, \theta_{m,n}$.

For the well separated frequency case, only the leading term of equation (3-31) exhibits a resonance for the n-quantum transition at $\omega = \frac{\omega_{ij}}{n} = \frac{E_i - E_j}{n\hbar}$. Thus the other terms of $a_{ij}^{(n)}(t)$ may be dropped for applied frequencies ω in the neighbourhood of $\omega \simeq \frac{\omega_{ij}}{n}$. This leads to

$$P_{i,j} \simeq \frac{\omega_1^2}{(\omega - \omega_o)^2} \sin^2 \left(\tfrac{1}{2} n (\omega - \omega_o)\tau\right) \qquad (3\text{-}32)$$

where $\omega_1 = \frac{2}{n} \sum_{\ell, m, \ldots r \ldots} \frac{A_{i\ell} A_{\ell m} \cdots A_{rj}}{(\omega_{\ell j} \mp (n-1)\omega)(\omega_{mj} \mp (n-2\omega)) \cdots (\omega_{rj} \mp \omega)}$

and, as above, $\omega_o = \frac{\omega_{ij}}{n}$.

When the oscillating field becomes large, the off-diagonal matrix elements can become as large as the diagonal matrix elements and perturbation theory is no longer reliable. Hack solves the Schrödinger equation, subject to the well-separated frequency condition, for the simplest case of two coupled angular momenta $I = J = \frac{1}{2}$. After integration by parts, the terms in the equations for the amplitudes of the states, which have large resonance denominators other than the initial or final ones for the transition in question, are dropped. Another term, a constant, is dropped

because, upon insertion into the equation for the amplitude of the final and initial levels, it is multiplied by a rapidly oscillating expotential thus tending to zero. A further approximation involves equating terms which are only equal for the case of exactly equally spaced levels. Hack then generalizes that solution to the case of two generally coupled angular momenta I and J. He obtains

$$P_{ij} \simeq \frac{\omega_1^2}{(\omega-\omega_o)^2+\omega_1^2} \sin^2\left(\tfrac{1}{2} n \left((\omega-\omega_o)^2+\omega_1^2\right)^{\frac{1}{2}} \tau\right) \qquad (3\text{-}33)$$

where ω_1 is as above in equation (3-32) but now ω_o (c.f. ω^* of equation (3-26) is defined by

$$\omega_o = \pm \frac{1}{n}\left(\omega_{ij} + \sum_{m_i-1} \frac{A_{\ell i}^2}{\omega_{i\ell}-\omega} + \sum_{m_\ell = m_i+1} \frac{A_{\ell r}^2}{\omega_{i\ell}+\omega} - \sum_{m_\ell = m_j-1} \frac{A_{\ell j}^2}{\omega_{i\ell}-\omega} - \sum_{m_\ell = m_j+1} \frac{A_{\ell j}^2}{\omega_{i\ell}+\omega}\right) \simeq \frac{\omega_{ij}}{n} \pm \mathcal{O}(b^2) \qquad (3\text{-}34)$$

The last four terms of the definition of ω_o indicate that, at increased r.f. amplitudes, the resonance frequency will not coincide exactly with the actual energy difference between the initial and final levels. It is clear that Hack and Salwen have obtained essentially the same expressions, and thus both theories predict the same behaviour of MQT as was discussed above.

5. Exact Solution

In order to solve the problem of MQT probabilities not subject to the limitations imposed by the theories discussed above, namely, that the

levels be either exactly equally spaced (Majorana and Salwen) or that the levels be quite unequally spaced (Salwen and Hack), R. G. Summers-Gill of the McMaster atomic beam group has proposed a nearly exact theory. Extensive use will be made of the interaction matrix and other relations developed in the first section of this chapter.

Starting with the interaction equation (3-13)

$$V(t)\Psi_m = \hbar b \left(\alpha_{m,m+1} \Psi_{m+1} e^{-i\omega t} + \alpha_{m,m-1} \Psi_{m-1} e^{+i\omega t} \right) \qquad (3\text{-}13)$$

and the total Hamiltonian, $\mathcal{H}$, given by

$$\mathcal{H} = \mathcal{H}_o + V(t),$$

the wave function $\Psi(t)$ at a time t during which the perturbation V(t) has been applied can be written as

$$\Psi(t) = \sum_{-F}^{F} C_m(t) \Psi_m \quad . \qquad (3\text{-}35)$$

Writing (t) in this manner means that states of different F are neglected. Typically $|\omega_{(F)} - \omega_{(F \pm 1)}| >> |\omega_{(m)} - \omega_{(m \pm m)}|_{\Delta F = 0}$ and such a simplification would appear to be entirely justified.

The Schrodinger equation for the system is

$$i\hbar \frac{\partial \Psi}{\partial t} = \mathcal{H}\Psi .$$

This condition leads to, using equation (3-35):

$$i\hbar \sum_{m=-F}^{F} \dot{C}_m(t) \Psi_m = \hbar \sum_m C_m \omega_{(m)} \Psi_m + \sum_m C_m(t)\, V(t) \Psi_m \qquad (3\text{-}36)$$

where the $\omega_{(m)}$ and Ψ_m were defined in equation (3-12). Using the definition of V(t), equation (3-36) becomes

$$i\hbar \dot{C}_m(t) = \hbar \omega_{(m)} C_m(t) + \hbar b \left(C_{m-1}(t)\, \alpha_{m-1,m}\, e^{-i\omega t} + C_{m+1}(t)\, \alpha_{m,m+1}\, e^{i\omega t} \right), \tag{3-37}$$

In order to remove the time dependence, new coefficients $a_m(t)$ are defined by

$$C_m(t) = e^{-im\omega t}\, a_m(t) \tag{3-38}$$

then $$-i\dot{a}_m(t) + (\omega_{(m)} - m\omega)\, a_m(t) + b\,(\alpha_{m-1,m}\, a_{m-1}(t) + \alpha_{m,m+1}\, a_{m+1}(t)) = 0 \ . \tag{3-39}$$

Equation (3-39) has solutions of the form $a_m(t) \propto e^{i\gamma t}$ provided that

$$(\gamma + \omega_{(m)} - m\omega)\, a_m(t) + b\,(\alpha_{m-1,m}\, a_{m-1}(t) + \alpha_{m,m+1}\, a_{m+1}(t)) = 0 \tag{3-40}$$

for all m in the range $-F \leq m \leq F$. For a non-trivial solution to the set of $2F+1$ coupled linear equations in $a_m(t)$, it is necessary that the determinant of equation (3-40) vanishes. Thus,

$$\begin{vmatrix} \gamma + \omega_{(-F)} + F\omega & b\,\alpha_{-F,-F+1} & 0 & 0 & \cdots \\ b\,\alpha_{-F,-F+1} & \gamma + \omega_{(-F+1)} + (F-1)\omega & b\,\alpha_{-F+1,-F+2} & 0 & \cdots \\ 0 & b\,\alpha_{-F+1,-F+2} & \gamma + \omega_{(-F+2)} + (F-2)\omega & b\,\alpha_{-F+2,-F+3} & \cdots \\ \cdot & \cdot & \cdot & \cdot & \cdot \\ \cdot & \cdot & \cdot & \cdot & \cdot \\ \cdot & \cdot & \cdot & \cdot & \cdot \end{vmatrix} = 0 \tag{3-41}$$

The $2F+1$ roots of (3-41) are denoted by γ_ℓ, where $1 \leq \ell \leq 2F+1$. The $a_m(t)$ can then be constructed as

$$a_m(t) = \sum_{\ell=1}^{2F+1} A_{m,\ell}\, e^{i\gamma_\ell t} \qquad (3\text{-}42)$$

Substituting equation (3-42) into equation (3-38) gives

$$C_m(t) = \sum_{\ell} A_{m,\ell}\, e^{i(\gamma_\ell - m\omega)t} \qquad (3\text{-}43)$$

The time independent coefficients, $A_{m,\ell}$, must satisfy the recursion relation

$$(\gamma_\ell + \omega_{(m)} - m\omega)\, A_{m,\ell} + b(\alpha_{m-1,m}\, A_{m-1,\ell} + \alpha_{m,m+1}\, A_{m+1,\ell}) = 0 \,. \qquad (3\text{-}44)$$

Equation (3-44) permits the calculation of transition probabilities in terms of coefficients $A_{m,\ell}$, which in turn depend upon the roots γ_ℓ. Now, a more convenient form of $|C_{m'}(t)|^2 = P_{m',m}$ will be given in terms of the $A_{m,\ell}$. From equation (3-43) $|C_m(t)|^2 = \left(\sum_\ell A^2_{m,\ell}\, e^{-i\gamma_\ell t}\right)^* \times$

$$\times \left(\sum_\ell A_{m,\ell}\, e^{-i\gamma_\ell t}\right)$$

But since $A^*_{m,\ell} = A_{m,\ell}$ as the $A_{m,\ell}$ are real, then

$$|C_m(t)|^2 = \sum_\ell A_{m,\ell}^{\,2} - 4 \sum_{\substack{\ell,\ell' \\ \ell > \ell'}} A_{m,\ell}\, A_{m,\ell'} \sin^2\left(\tfrac{1}{2}(\gamma_\ell - \gamma_{\ell'})t\right) . \qquad (3\text{-}45)$$

There are $2F+1$ magnetic substates $m_1, m_2, \ldots m_{2F+1}$. For definitness, assume that at $t = 0$ the system of $2F+1$ m levels is in the state m_1, then the probability, after the perturbation $V(t)$ has been applied for a time $t = \tau$, that the system will have made a transition

to a state m_2, is $\left| C_{m_2}(\tau) \right|^2$. Because it was assumed that, at $t = 0$, the system was in the state $m = m_1$, then

$$\sum_{\ell} A_{m,\ell} = \delta_{m,m_1} \quad . \tag{3-46}$$

The probability of a transition having been made from m_1 to m_2 at the time $t = \tau$, is, therefore

$$P_{m_2,m_1} = \left| C_{m_2}(\tau) \right|^2 = \delta_{m_1,m_2} - 4 \sum_{\substack{\ell,\ell' \\ \ell\ \ell'}} A_{m_2,\ell} A_{m_2,\ell'} \sin^2\left(\tfrac{1}{2}(\gamma_\ell - \gamma_{\ell'})\tau\right) . \tag{3-47}$$

To evaluate the required coefficients $A_{m,\ell}$, use is made of the recursion relation they satisfy (equation (3-44)). For this purpose, a set of parameters Δ_m^q is defined as

$$\Delta_m^q = \sum_{\ell} (\gamma_\ell)^q A_{m,\ell} \quad . \tag{3-48}$$

Thus, for the initial level being m_1, it follows

$$\Delta_m^0 = \sum_{\ell} A_{m,\ell} = \delta_{m,m_1}$$

$$\Delta_m^1 = \sum_{\ell} (\gamma_\ell)^1 A_{m,\ell} = (m\omega - \omega_{(m)})\, \delta_{m,m_1} - b\,(\alpha_{m-1,m}\ \delta_{m-1,m_1} + \alpha_{m,m+1}\ \delta_{m+1,m_1})$$

$$\vdots$$

$$\Delta_m^q = \sum_{\ell} (\gamma_\ell)^q A_{m,\ell} = (m\omega - \omega_{(m)})\, \Delta_m^{q-1} - b(\alpha_{m-1,m}\ \Delta_{m-1}^{q-1} + \alpha_{m,m+1}\ \Delta_{m+1}^{q-1}) \quad . \tag{3-49}$$

The relation (3-49) is expressed as $\sum_{\ell} (\gamma_\ell)^q A_{m,\ell} = \Delta_m^q$ which is a system

of $2F+1$ equations which can be solved for the coefficients $A_{m,\ell}$. One method of effecting a solution is given by Kramer's Rule which yields

$$A_{m,\ell} = \frac{D_\ell(m,m_1)}{J} \tag{3-50}$$

where

$$J = \begin{vmatrix} 1 & 1 & \cdots & 1 \\ \gamma_1 & \gamma_2 & & \gamma_{2F+1} \\ \gamma_1^2 & \gamma_2^2 & & \gamma_{2F+1}^2 \\ \gamma_1^3 & \gamma_2^3 & & \gamma_{2F+1}^3 \\ \cdot & & & \cdot \\ \cdot & & & \cdot \\ \cdot & & & \cdot \\ \gamma_1^{2F} & \gamma_2^{2F} & & \gamma_{2F+1}^{2F} \end{vmatrix}$$

and

$$D_\ell(m,m_1) = \begin{vmatrix} 1 & \cdots & 1 & \Delta_m^0 & 1 & \cdots & 1 \\ \gamma_1 & & \gamma_{\ell-1} & \Delta_m^1 & \gamma_{\ell+1} & & \gamma_{2F+1} \\ \cdot & & \cdot & \cdot & \cdot & & \cdot \\ \cdot & & \cdot & \cdot & \cdot & & \cdot \\ \cdot & & \cdot & \cdot & \cdot & & \cdot \\ \gamma_1^{2F} & \cdots & \gamma_{\ell-1}^{2F} & \Delta_m^{2F} & \gamma_{\ell+1}^{2F} & \cdots & \gamma_{2F+1}^{2F} \end{vmatrix}.$$

Thus, in terms of the quantities

$$P_{m_1,m_2} = \delta_{m_1,m_2} - \frac{4}{J^2} \sum_{\substack{\ell,\ell' \\ \ell\ \ell'}} D_\ell(m_2,m_1)\, D_{\ell'}(m_2,m_1) \sin^2\left(\tfrac{1}{2}(\gamma_\ell - \gamma_{\ell'})\tau\right) \tag{3-51}$$

The transition probability from m_1 levels other than m_2 follows immediately from equation (3-51), the terms $D_\ell(m_2,m_1)$ being replaced by $D_\ell(m,m_1)$. All this means is that, instead of using the vector $\Delta^q_{m_2}$ in forming $D_\ell(m_2,m_1)$, a different Δ^q_m is selected, the one selected being appropriate to the final level m. Of course, different initial conditions also change the vectors Δ^q_m.

This derivation is an exact treatment of the MQT probability problem except for the neglect of the following:

(1) counter rotating components of the oscillating field

(2) contributions to MQT probabilities from states of different F

(3) spatial variations of the oscillating field amplitude.

CHAPTER IV

APPARATUS, EXPERIMENTAL TECHNIQUE AND COMPUTER PROGRAMMES

The McMaster atomic beam apparatus used in these experiments is of conventional "flop-in" design. It has been described in detail elsewhere (King, 1960; Cameron et al., 1962). The discussion of the apparatus will here be limited to those aspects particularly pertinent to the experiments reported. Descriptions of computer programmes based on the expressions developed in Section (III-4) will also be given below.

1. Operation of the Apparatus

Figure 5 is a schematic representation of the apparatus. Source material is evaporated in an oven, O. It emerges through slits in the face of the oven in the form of an atomic beam. Various beam collimating slits are shown. Atoms in the beam pass in succession through the three magnetic fields of the magnets denoted A, C and B. The A and B magnets are strong, deflecting magnets with fields and gradients perpendicular to the centre line of the apparatus. The C magnet produces a weak, static, uniform, variable intensity field whose direction defines the Z axis. The C field causes a Zeeman splitting of the atomic hyperfine multiplets. Transitions are induced between these magnetic substates by a small magnetic dipole antenna (not shown) situated in the gap of the C magnet. Atoms are detected by a conventional surface ionization detector called a "hot wire". This is denoted HW in Figure 5. An obstacle wire, called a "stop wire", S, prevents atoms which are undeflected by the A and B magnets from

Figure 5

Schematic Diagram of Apparatus

Atoms which have not made transitions involving m_J (in A field) $= -m_J$ (in B field) suffer two successive deflections in the same direction and are not focussed.

HW
B
S
C
O
A
HA
H
O

reaching the hot wire. The apparatus is evacuated by fractionating oil diffusion pumps to a pressure of about 10^{-6} mm Hg. This effectively eliminates beam scattering from residual gas in the apparatus. The beam path from the oven to the hot wire is about 1 m which, for the width of collimating slits used (0.25 mm), gives an overall transmission efficiency of about 10^{-4}.

2. Beam Production

The source material used was metallic sodium. An illustration of the tantalum source oven is given in Figure 6. The slit jaws form an exit channel about 0.25 mm wide, 0.75 cm high and 0.25 cm deep. The depth of the slit provides a modicum of beam collimation. The oven was indirectly heated by passing current through tungsten filaments situated near the oven. Once the filament current was set and the oven permitted to come to thermal equilibrium, the long term beam intensity usually varied no more than ± 5%.

3. Magnet System and Magnetic Focusing

The C magnet is energized by a current regulated power supply. The stability of the supply current is approximately 1 part in 10^4. The intensity of C field is continually variable in range from 0 to about 500 gauss. No large drifts in C field intensity are attributable to variations in the output current of C magnet supply. However, variations of C field intensity did occasionally occur and these were attributed to variations in the intensity of the fringing field from the A and B magnets. The current regulated power supply feeding the high impedance A and B magnets was capable of supplying 2 amperes at 2000 volts. For these experiments, a current of

Figure 6

Oven

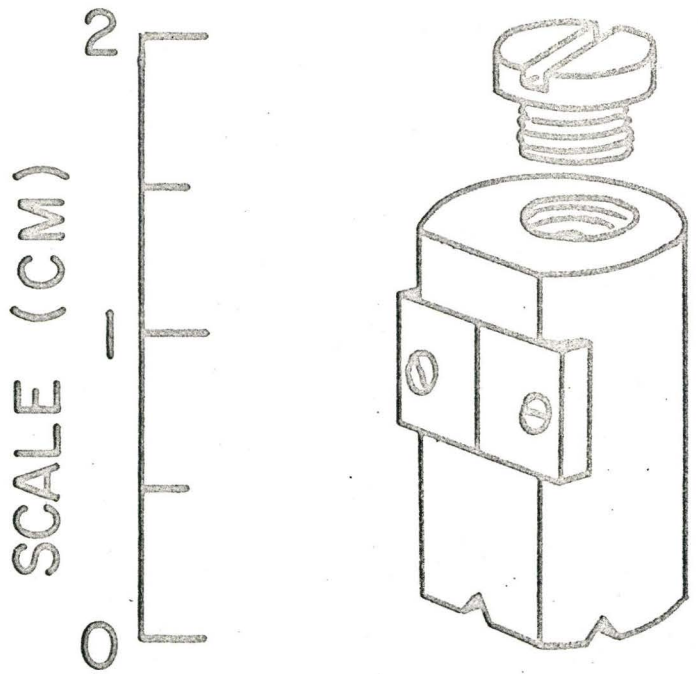
SCALE (CM)
0
1
2

1 ampere was used. The stability of the A and B magnet supply was about 1 part in 1000. This current produced A and B fields of 5 and 10 kilogauss respectively.

In the A and B fields, paramagnetic atoms are subjected to the Paschen-Bach effect. Because those magnets produce large field gradients, atoms experience a transverse force

$$\vec{F} = -\nabla V = -\frac{\partial V}{\partial H}\nabla H$$

$$= m_J \mu_o g_J \frac{\partial H}{\partial Z}\hat{Z} \qquad (4\text{-}1)$$

where m_J is the Z component of the total electronic angular momentum and $\hat{Z}$ is a unit vector along the Z axis. The A and B field gradients are parallel, thus, atoms which have the same sign of m_J in both these fields experience two deflections in the same direction. These atoms miss the exit aperture and are not ionized by the hot wire. However, atoms which have changed their sign of m_J because they were induced to make appropriate Zeeman transitions in the C field region are focussed upon the exit aperture in front of the hot wire. For a suitable choice of geometry, it is possible, for a wide range of velocities, to focus onto the exit aperture all atoms which have made transitions of the type m_J (in A field) = $-m_J$ (in B field). In Na^{23} (c.f. Figure (1)), it is seen that all focusable $\Delta F = 0$ transitions involve the $|(2), -2\rangle$ state as either final or initial state. Thus, only four MQT are observable in Na^{23} with the apparatus at this laboratory.

4. Hot Wire Detection System

The hot wire surface ionization system works on the principle that a fraction of the atoms evaporated from a hot surface are emitted as ions if

the ionization potential of the atom is lower, or not much larger, than the work function of the hot surface. The hot surface was provided by a 0.2 mm diameter tungsten wire resistance heated to about 1600°C. The hot wire is mounted vertically to intercept atoms leaving the B magnet exit slit. Ions created at the hot wire surface are collected on a nichrome strip and the resulting ion current is measured on a Victoreen-Tullamore electrometer (Model VTE-2). In order to have maximum utilization of the ions created at the hot wire surface, an electrostatic potential is maintained between the hot wire and the collector.

The hot wire mount is capable of being moved in an arc. This permits the hot wire to be positioned within a band extending left and right of the geometrical centre line of the apparatus. This flexibility is required to accommodate the small changes of apparatus alignment which occur over a period of time. It also proved to be useful in monitoring the Na beam intensity.

The hot wire detection system has a small inherent background current. In addition, there was usually a larger background current due to atoms scattered from the beam landing on the hot wire producing a current. The latter background is extremely dependent upon the pressure of the apparatus. In the experiments performed, it was required to subtract off the background, hence several determinations of the background level were required during the course of the experiment. This determination of the background is known as an "r.f. off" measurement.

The response of the hot wire detection system was checked by raising the beam intensity so that the electrometer reading was a factor of ten over

a previous value. The variation of intensity of resonance as a function of applied r.f. signal amplitude was compared for both beam intensities. The relative changes of resonance intensity with respect to r.f. amplitude were the same in both cases indicating that the hot wire electrometer system's response was linear.

It is necessary in ABMR experiments to monitor changes in the beam size. Normally, this is done by removing the obstacle wire so that the intensity of the undeflected portion of the beam can be recorded. Such a procedure is known as the "half-beam" method. However, because of the large deflections which Na atoms experience in the A and B fields, the "half-beam" intensity is of the order of the background noise of the hot wire detection system. Recourse was then made to the large "thrown-out" beam produced by the deflecting magnets. Figure 7 shows the profile of paramagnetic atoms comprising the beam. The beam size was monitored by setting the hot wire to the thrown-out portion of the beam profile (labelled "Monitor" in Figure 7) and recording any changes in intensity. No large scale variations (i.e. greater than 10%) were noted in beam intensity.

5. Radio-Frequency Equipment and Use

The experiments performed were measurements of the intensity of a MQT at resonance frequency as a function of the r.f. field amplitude, H_o. This required a means of precisely varying the r.f. amplitude. For this purpose, precision attenuators were used. The use of attenuators further required that a means of matching the load to line be used, otherwise the attenuators would not function properly. Figure 8 is a block diagram of the r.f. equipment layout used in these experiments.

Figure 7

Thrown-out Beam

The data is for Cs^{133}. However, for Na^{23}, the shape of the beam profile is little changed.

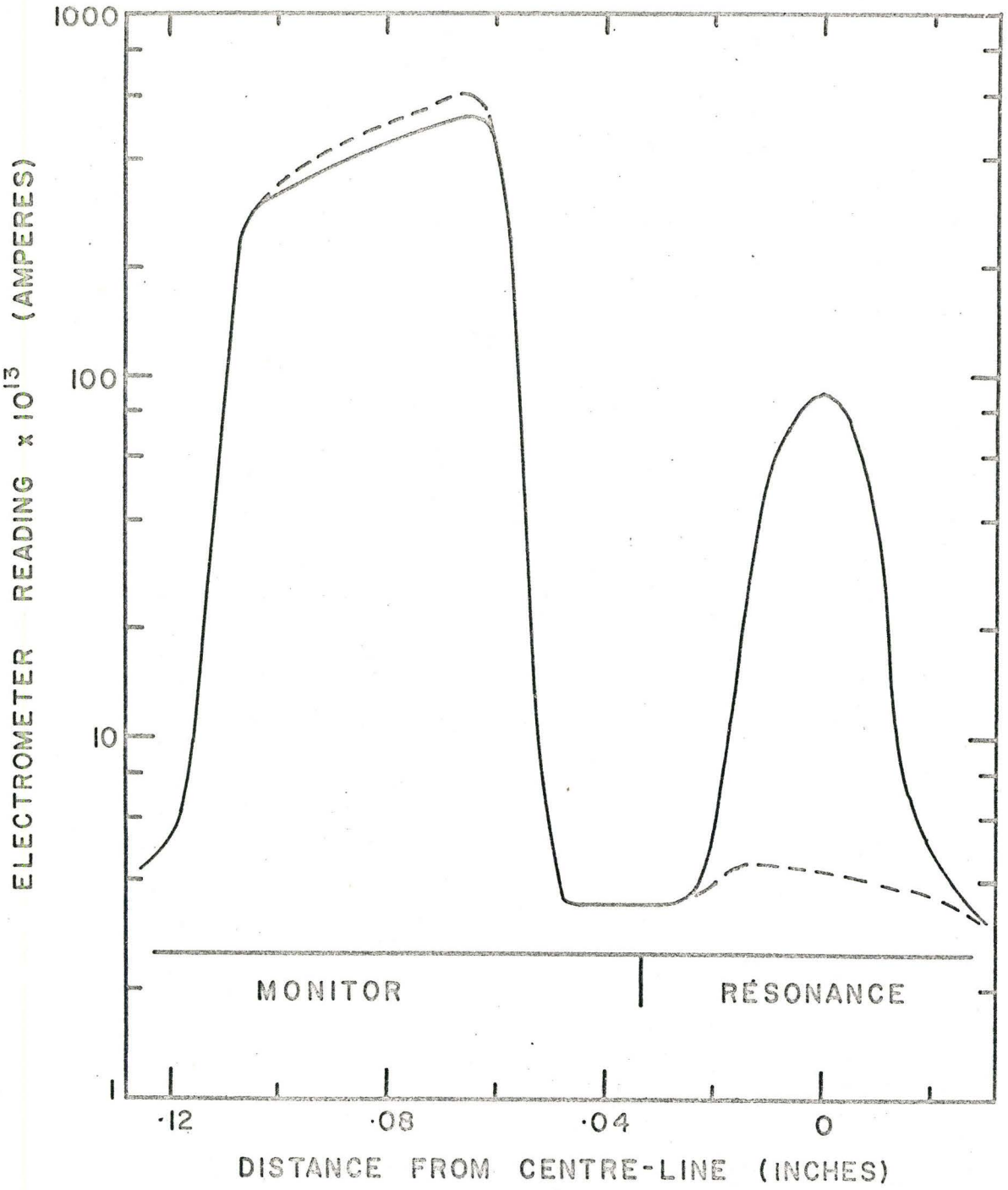
1000
100
10
1
ELECTROMETER READING x 10^13 (AMPERES)
MONITOR
RÉSONANCE
·12
·08
·04
0
DISTANCE FROM CENTRE-LINE (INCHES)

Figure 8

Block Diagram of Radio-Frequency Equipment

The components are indicated by the following abreviations:

Oscillator -	Osc
Amplifier -	Amp
Attenuator -	Attn
Directional Coupler -	D C
Crystal Detector -	Xtal
Oscilloscope -	Scope
Doubler Stub Tuner -	DST
Frequency Converter -	CNVTR
Frequency Counter -	Counter .

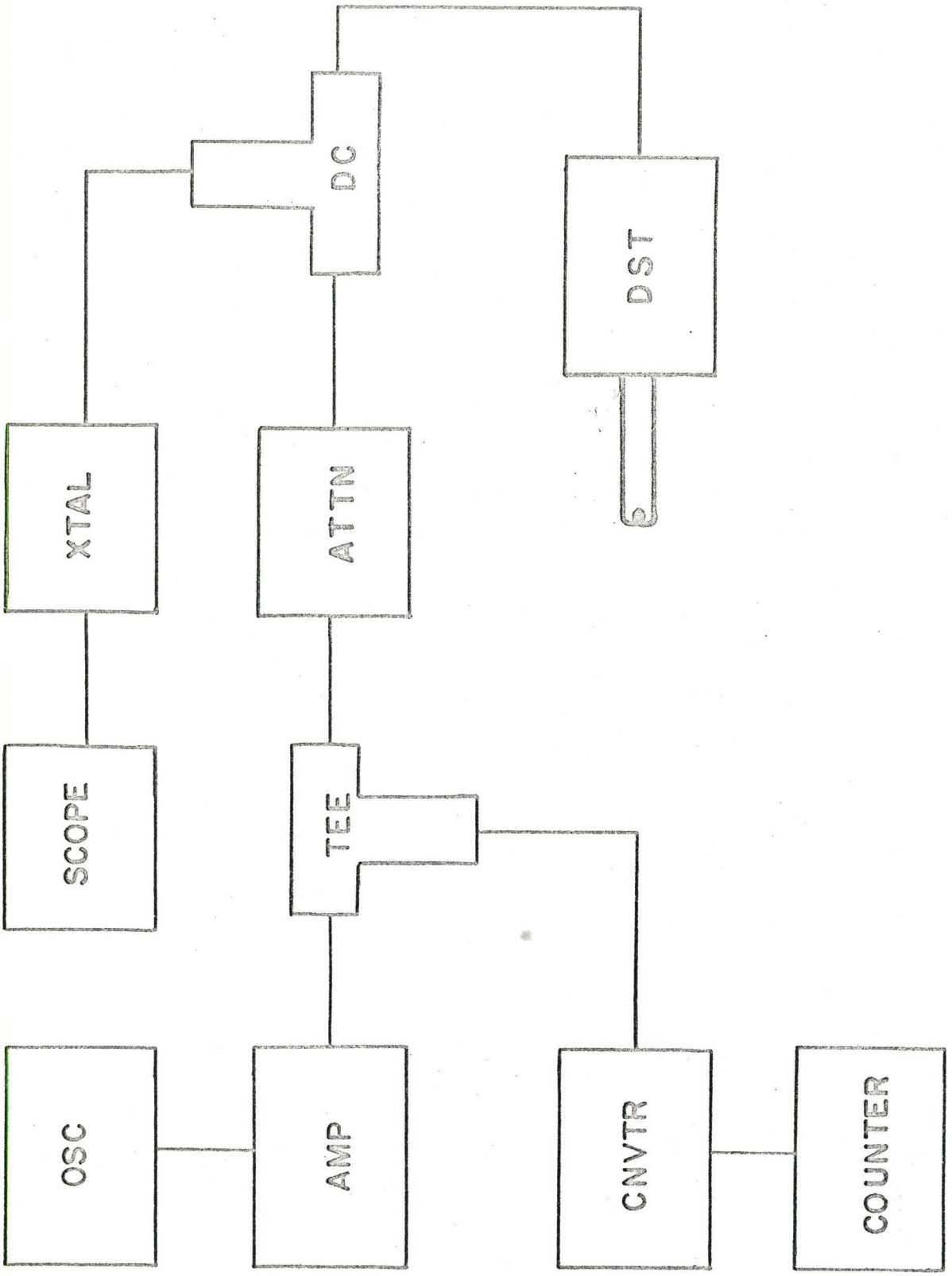
DC
DST
XTAL
ATTN
SCOPE
TEE
OSC
AMP
CNVTR
COUNTER

The dipole antenna used to induce the MQT, commonly called a "hairpin", is a U-shaped length of 20-gauge copper wire terminating a section of co-axial cable. The loop is oriented within the C magnet gap so that its magnetic field is parallel to the beam axis and perpendicular to the direction of the C field. A typical VSWR for the loop alone was $\simeq 15 : 1$. A double stub tuner was used to match the "hairpin" to the line so that the attenuator would be working into its characteristic impedance. The tuner used was a Weinschel Engineering Company DS-109H which is specifically designed to permit easy matching in the frequency range of 40 to 400 Mc/sec. Co-axial cable connecting the r.f. components was type RG-8/U which has constant impedance from D.C. to $\sim$ 1 kMc/sec. The connectors used offered the same wide range response. Table 1 is a list of the radio-frequency equipment used.

The principle of operation of the r.f. system is as follows. The r.f. signal is (if required) amplified and a very small fraction of it is drawn off to obtain its frequency, using the frequency counting system. The attenuator is matched to the load by adjusting the stub length of the double stub tuner. This is accomplished using the directional coupler which is arranged in the line so that it only detects energy reflected from the load. The reflected signal is detected, using a crystal diode, and viewed on a sensitive oscilloscope. During the matching procedure only, the r.f. signal is square wave modulated at 1 kc/sec. The stubs are adjusted until the square wave pattern on the oscilloscope flattens into a horizontal line, indicating that no energy is being reflected into the attenuator. Prior to matching, the load presented a bad mis-matching, hence the matching usually

TABLE I

Radio-Frequency Equipment

Item	Manufacturer	Model	Comments
VHF Oscillator	Wandel and Goltermann	LMS-68	Using plug in units, the oscillator covers the frequency range 4 to 1000 Mc/sec. Depending on plug in unit used, the output is 1 or 0.5 watts into 60 ohms
VHF Amplifier	Boonton Radio Corporation	230-A	The amplifier covers the frequency range from 10 to 500 Mc/sec. Its output is nominally rated at 4 watts into 50 ohms.
Tee (Adjustable Attenuator)	General Radio Company	874-AG	The "drawn-off" portion's amplitude is $\simeq$ -20 db that of "straight-through" portion.
Directional Coupler	M. C. Jones Company (Micro-Match)		Used to sample the amplitude of waves reflected from load.
Crystal Detector	Telonic Company	XD-23E	Used to detect reflected waves sampled by directional coupler.
Frequency Converters	Beckmann Company	7570-Amplifier 7571, 7572, 7573 Converter units	The frequency counting system has an overall stability of 1 part in 10^6
Frequency Counter	Beckmann Company	7170	
Double Stub Tuner	Weinschel Engineering Company	DS-109H	The double stub tuner is specially designed to cover the frequency range of 40 to 400 Mc/sec.

slightly changed the operating frequency of the r.f. system. For this reason, the oscillator was again reset to the desired frequency and, if required, the stubs readjusted. This process was repeated until satisfactory matching was obtained. A VSWR of 1.1 was usually easily obtained using this procedure. Through the use of various lengths of co-axial cable inserted into the line between the tuner and load, the feasible matching was extended down to ~ 20 Mc/sec.

The calibration of the variable attenuator was checked using a General Radio Company 1223 narrow band amplifier in logarithmic mode.

6. General Experimental Procedure

These experiments consisted in determining the power dependence of MQT at MQT resonance frequency. Before an experiment was begun, the desired C field intensity was chosen. Then the nominal resonance frequencies for that field were determined. For this purpose, it was convenient to use a graph which gave the nominal frequencies as a function of C field intensity, such as the one in Figure 2. The C field setting was adjusted until a 1-quantum resonance was observed at the frequency corresponding to desired field. The 2, 3 and 4-quantum transitions generally required use of the VHF amplifier. Then the peak resonance frequency was found for a desired MQT. The r.f. system was then matched to the load at the peak frequency using the double stub tuner. Finally, the resonance intensity at the peak frequency was recorded for different values of attenuator setting. During the course of the run, the frequency of the 1-quantum transition was checked to assure that the resonance had not shifted due to drift of either the C field or the fringing A and B fields. If a shift was noted,

that set of data was discarded. All points were repeated at least twice and most were repeated three times. At the beginning and end of each run, the beam intensity was checked by positioning the hot wire so as to intercept the thrown-out position of the beam. Because it was required to subtract off the background level, several "r.f.-off" measurements were made during the course of a run. Any variations in beam intensity or background were linearly interpolated and the appropriate corrections were made. To eliminate, as far as possible, the effects of systematic drift, values of attenuation were chosen at random.

In all, 31 determinations of the r.f. amplitude dependence of MQT transition intensity at MQT resonance frequency were made. These runs were conducted over a wide range of static field values and, thus, for a wide variety of degrees of departure of the levels from equal spacing. The impedance matching system was, thus, operated at several different frequencies, largely removing any systematic distortion in the data caused by the tuners. For the lowest value of C field intensity used (corresponding to X = 0.05), the various MQT were separated by ~ 0.25 Mc/sec. Typically, the FWHM of the 1-quantum transition, the "widest" of the MQT, is ~ 150 kc/sec. Thus, all observed resonances were well defined.

The typical signal to noise ratio, for the resonance at peak intensity, was $\simeq 15 : 1$.

The error associated with the electrometer reading was estimated to be $\pm$ 1/2 scale division. This error combines both scale reading error and the random fluctuations appearing in the electrometer's output. Of course, this error is compounded when the background is subtracted off. For n readings of

the same point, the error was divided by $\sqrt{n}$ and the values averaged.

7. Computer Programmes

The expression for MQT probabilities, developed in Section (III-4), was programmed for the McMaster IBM 7040 computer using "FORTRAN IV" language. In all, three versions of the same basic programme were written. These programmes are denoted as MQTSLV, HUNT and SHIFT.

The programme MQTSLV calculated all five orders of MQT probabilities from the probability for no transition $|2, -2\rangle \rightarrow |2, -2\rangle$, to the 4-quantum transition involving the states $|2, -2\rangle \rightarrow |2, 2\rangle$. These five transition probabilities were calculated for predetermined choices of the r.f. amplitude parameter b and the applied frequency of the oscillating field ω. The input variables for MQTSLV were

(1) the energies of the magnetic substates $\omega_{(m)}$ (in units of Mc/sec)

(2) the matrix elements $\alpha_{m,m'}$ (dimensionless)

(3) the applied frequency ω (Mc/sec)

(4) the r.f. amplitude parameter b (Mc/sec) which was incremented in steps of Δb (Mc/sec)

(5) the length of time that the system is perturbed by the oscillating field τ (10^{-6} sec).

Values of $\omega_{(m)}$ and $\alpha_{m,m'}$ were obtained for the desired value of static field from a programme written by G. M. Stinson. This programme, denoted as ALPHA, uses both the Breit-Rabi equation to find the energies $\omega_{(m)}$ (equation (2-9)) and formulae given by Salwen (Salwen, 1956) to find the matrix elements $\alpha_{m,m'}$.

The first four of the input variables, namely $\omega_{(m)}$, $\alpha_{m,m'}$, ω, and b, are required to evaluate the roots γ_ℓ. Use was made of a library subroutine of the McMaster installation which finds the eigenvalues of symmetric matrices. The negatives of the eigenvalues so obtained were the roots $\gamma\ell$.

Next, the matrices Δ_m^q and $\sum_\ell \gamma_\ell^q$ were calculated from equation (3-48).

Having stored in two two-dimensional arrays the matrices Δ_m^q and $\sum_\ell \gamma_\ell^q$, the coefficients $A_{m,\ell}$ are found by solving the five linear equations $\sum_\ell A_{m,\ell}\gamma_\ell^q = \Delta_m^q$ for the $A_{m,\ell}$. To do this use was made of another library subroutine which permits the solution of a large number of simultaneous linear equations.

Having found the coefficients $A_{m,\ell}$, the transition probability (equation (3-47)) $P_{m,m''} = \delta_{m,m'} - 4 \sum_{\substack{\ell,\ell' \\ \ell>\ell'}} A_{m,\ell} A_{m,\ell'} \sin^2 (\tfrac{1}{2}(\gamma_\ell - \gamma_{\ell'})\tau)$ is found. The indicated summation is performed in the usual manner. It is in this last step that use is made of the final input datum τ.

The five MQT probabilities $P_{m,-2}$ (m = -2, -1 ... 2) are then printed. Then the calculation is repeated for the incremented value of b. This process of incrementing b continues for a predetermined number of times. Then a new value of ω is read in and the b- looping resumes at the new value of ω. This continues for the desired number of frequencies and then the programme is terminated.

Criteria exist which enable checking the validity of the calculation. In the limit of small x, MQT probabilities calculated by this method must converge to the transition probabilities given by the Majorana formula.

Also, for all x, the sum of all transition probabilities — including the "no-transition" probability $|(2), -2\rangle \leftrightarrow |(2), -2\rangle$ — must be unity. Finally, for finite x and small values of r.f. amplitude, the calculated resonance frequency must be very close to nominal n-quantum resonance frequency, $\omega_n = \frac{|E_f - E_i|}{n\hbar}$. This is because the perturbation theory arguments of Salwen and Hack must hold for the case of well separated resonances. Thus, using Salwen's result, equation (3-26) $\omega^* = \omega_{nominal} + O(b^2) \rightarrow \omega_{nominal}$ for small b. For the case of exactly equal spacing of the levels, the Majorana formula predicts no resonance shifts no matter how large b becomes.

After it had been established that MQT SLV was giving results in conformity with the criteria established above, HUNT and SHIFT were written.

The programme HUNT automatically obtains a rough value of "optimum b" for a desired MQT and then plots the transition's line shape at that value of b. Using the information obtained from HUNT so that one knows what sort of values of b are required to give reasonably large transition probabilities, SHIFT is next used.

The programme SHIFT calculates and plots the resonance line shape for any desired values of b and any range of applied frequencies. Usually the computer would take approximately 0.5 seconds to find the MQT probability for a given b and ω. Occasionally, for values of $x \simeq 0.02$, the eigenvalue subroutines became trapped in a loop. When this happened, no output was obtained and then, after 10 minutes, the programme was terminated.

8. Velocity Averaging

In ABMR, atoms forming the beam possess a velocity distribution

$$I(v) = \frac{2I_o}{\alpha^4} v^3 e^{-v^2/\alpha^2} dv \qquad (4\text{-}2)$$

where $I(v)$ is the beam intensity for atoms in the velocity range v to $v + dv$, I_o is the full beam intensity, and α is defined by $\alpha = \sqrt{\frac{2kT}{m}}$, where k is Boltzmann's constant, T is the temperature of the source in ^oK, and m is the mass of atoms forming the beam. Equation (4-2) means that atoms in the beam are subjected to the perturbation $V(t)$ for various lengths of time, $t = \frac{\ell}{v}$ where ℓ is the extent of the oscillating r.f. field.

Thus, it is common practice in ABMR transition probability calculations to average the transition probability with respect to time over all the velocities of the atoms comprising the beam. This is indicated by

$$\overline{P_{m,m'}} = \int_o^\infty I'(t) P_{m,m'}(t) dt \qquad (4\text{-}3)$$

where $I'(t)$ is the velocity distribution $I(v)$ written in terms of the time t and $P_{m,m'}(t)$ is the transition probability appropriate to the transition involved. Tabulated expressions exist for $\overline{P_{m,m'}}$ using, as $P_{m,m'}(t)$, the Rabi transition probability.

$$P_{\frac{1}{2},-\frac{1}{2}} = \frac{(2b)^2}{(\omega_o - \omega)^2 + (2b)^2} \sin^2\left(\tfrac{1}{2}((\omega_o - \omega)^2 + (2b)^2)t\right). \qquad (3\text{-}18)$$

For cases in which $P_{m,m'}(t)$ is not an analytic expression, as is the case for the expressions developed in Section (III-5), numerical

methods are required to perform the velocity averaging.

One way of doing this is to calculate the velocity averaged transition probability $\bar{P}_{m,m'}$, using

$$\bar{P}_{m,m'} = \sum_{j=1}^{N} P_{m,m'}(t_j)\, I(v_j) \qquad (4\text{-}4)$$

where N is the number of points taken to obtain the velocity distribution, t_j is the time corresponding to the j^{th} value of velocity v_j, and $P_{m,m'}(t_j)$ is the MQT probability for the time t_j.

A particular effect velocity averaging has on resonance line shapes is to reduce the intensity of subsidiary maxima occurring at frequencies $\nu \neq \nu_o$. Such subsidiary maxima are evident in Figure 3. For values of b not too much larger than b_{opt}, the velocity averaged transition probability possesses only a single maximum. Another effect of velocity averaging is to reduce the depth of the drop in transition probability that MQT exhibit for certain values of b b_{opt}. This is evident in Figure 4 using the Majorana expression.

In the early stages of this work, a programme incorporating a 5-point velocity average was used to calculate MQT probabilities. The programme was denoted as MQT 5. It was found that when the mean time of MQT 5 equalled the single value of time used in MQTSLV and for values of $b \lesssim b_{opt}$, the transition probabilities of the two programmes where essentially unchanged.

For this reason and in order to reduce the length of computer runs, velocity averaging was not employed any further in this work. All computed data presented are for a single value of time, t = 4 microseconds.

CHAPTER V

EXPERIMENTAL AND THEORETICAL RESULTS

In this chapter, the results of the power dependence experiments on Na^{23} are presented. Comparison will be made between the theory developed in Section (III-5) and the results of the power dependence experiments. Finally, theoretical results pertinent to the behaviour of MQT for various degrees of departure of their levels from equal spacing will be given.

1. Power Dependence Experiments and Calculations

Typical MQT resonance line shapes for Na^{23} are presented in Figure 9. The relatively large width of the 3 and 4-quantum transition resonance line shapes is almost certainly due to inhomogeneities of the C field. It is seen that there are apparently no large scale alterations of the resonance line shapes for the various values of x shown in Figure 9.

The power dependence experiments were performed at frequencies appropriate to the frequency peaks of the resonance line shapes. Typical results of these experiments are shown in Figures 10. Having mentally drawn in lines connecting the points of Figures 10, one would note the following effects concerning the (thus formed) experimental power dependence curves. For a particular transition multiplicity, there are no large variations in the shapes of the experimental power dependence curves for different values of x. However, as transition multiplicity changes, the shapes of the experimental power dependence curves are quite different

Figure 9

Resonance Line Shapes

The numbers indicate transition multiplicity. The dashed horizontal line indicates the background noise. The The values of x are given to the nearest hundredth. No value of x is indicated for the 1 and 2-quantum resonances at 32. and 31.5 mc/sec. because, to the nearest hundredth, it is 0.07. Thus, the 4-quantum transition of the lower left graph and these 1 and 2-quantum transitions are at practically, but not exactly, the same fields.

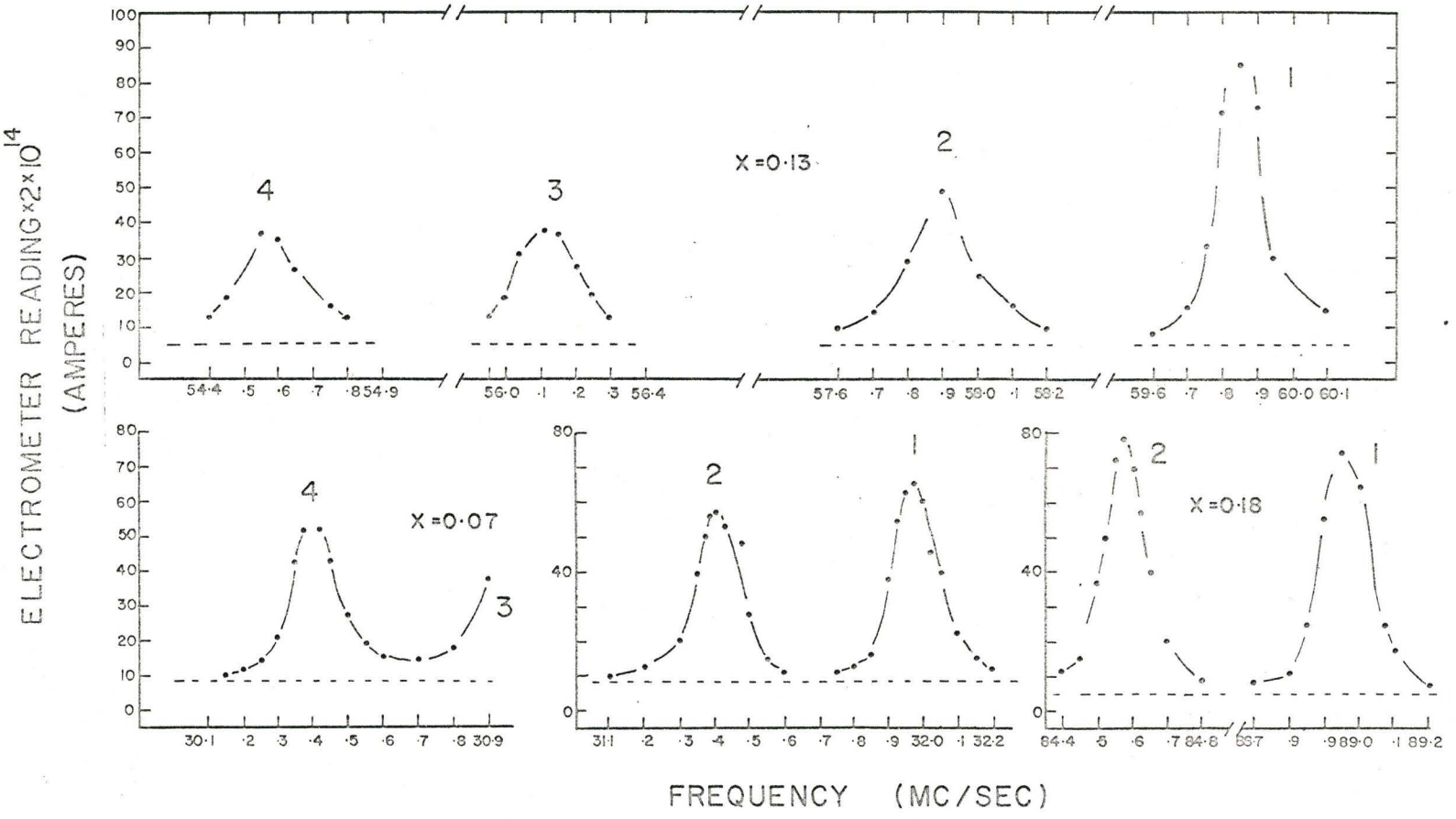
ELECTROMETER READING×2×10^14
(AMPERES)
X=0·13
X=0·07
X=0·18
4
3
2
1
FREQUENCY (MC/SEC)

Figures 10-a, b, c and d

Experimental Power Dependence Data

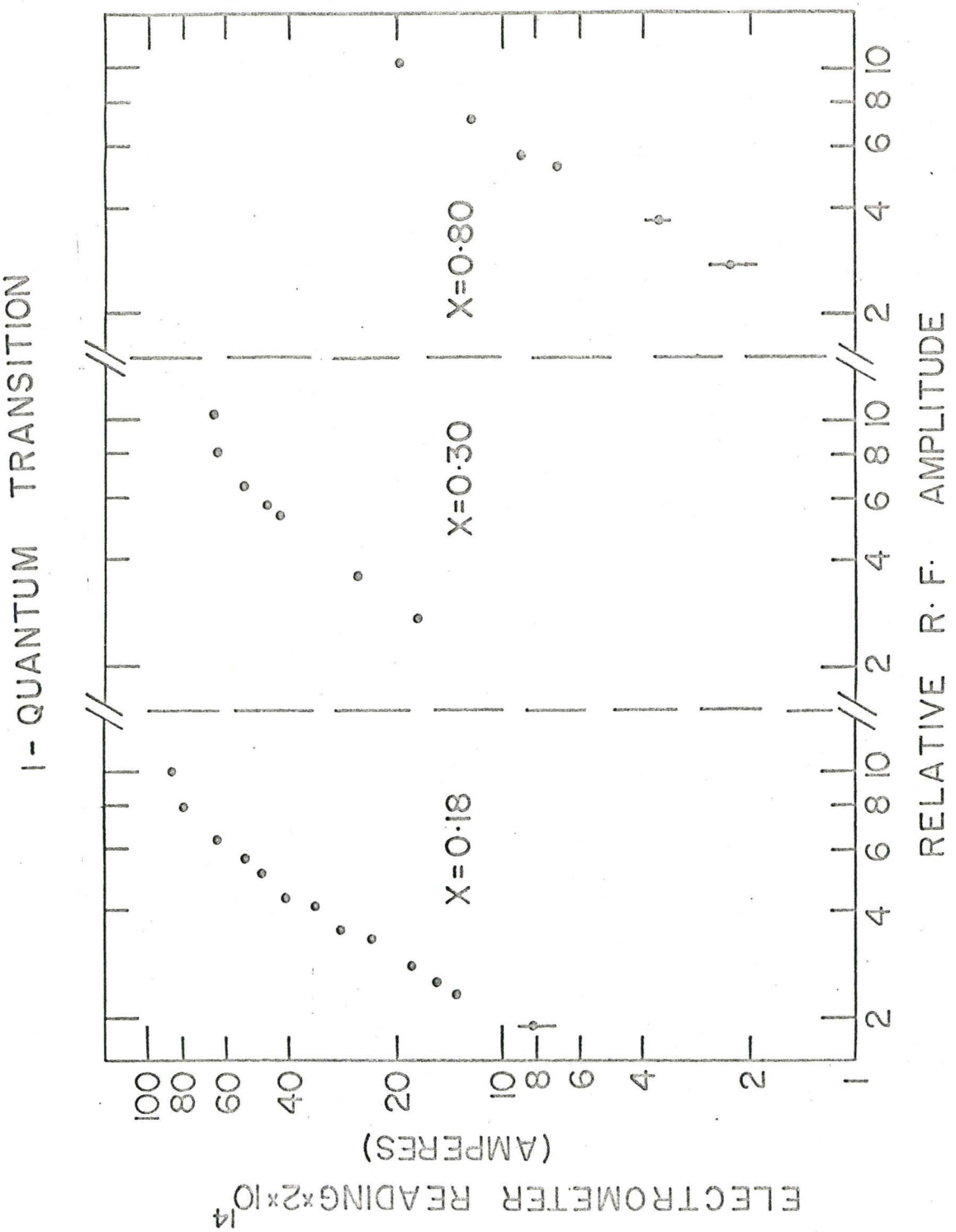
1-QUANTUM TRANSITION
X=0·18
X=0·30
X=0·80
ELECTROMETER READING ×2×10⁻¹⁴
(AMPERES)
RELATIVE R·F· AMPLITUDE

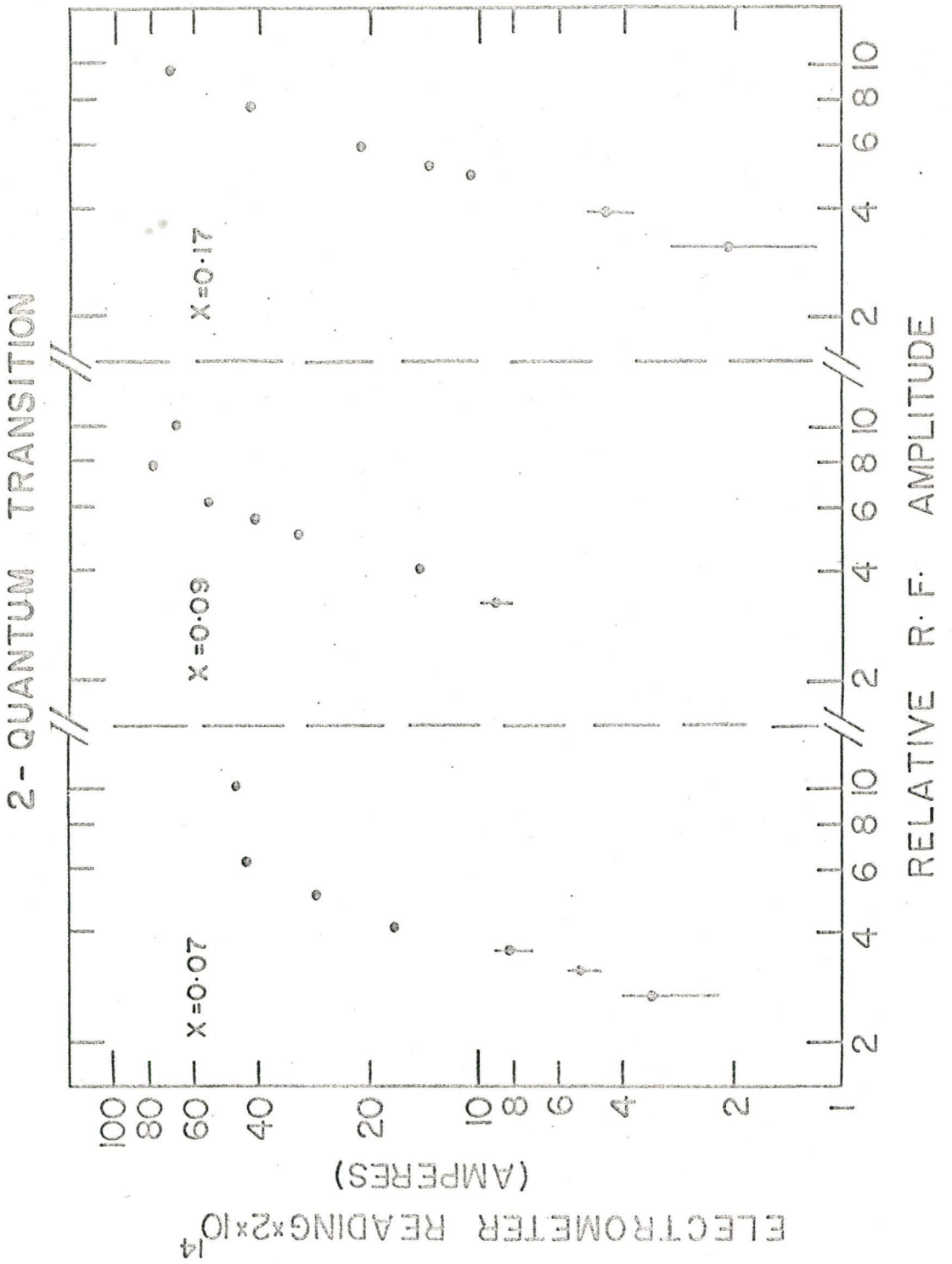
2 - QUANTUM TRANSITION
x=0·07
x=0·09
x=0·17
ELECTROMETER READING ×2×10⁻¹⁴
(AMPERES)
RELATIVE R.F. AMPLITUDE

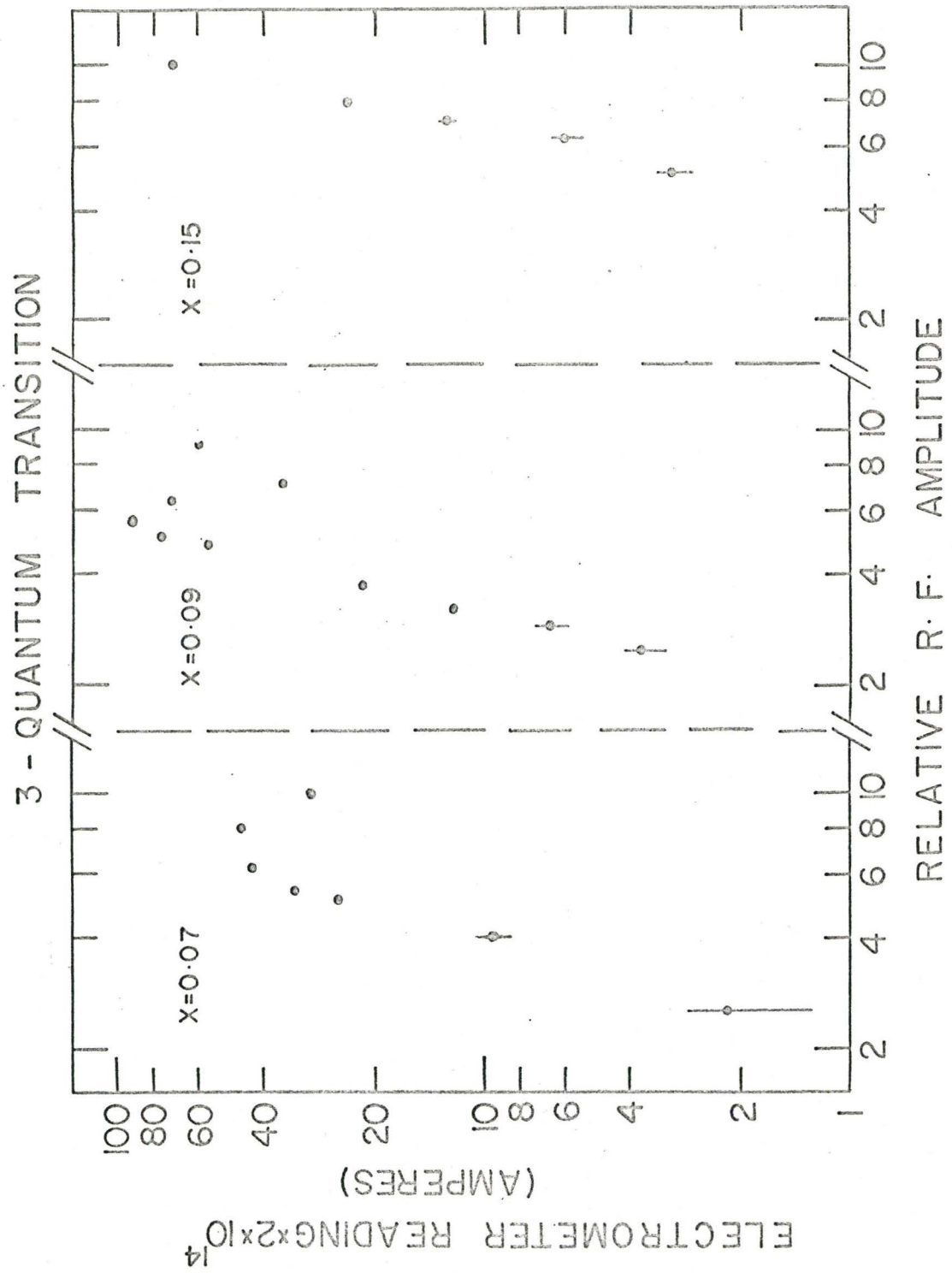
3 - QUANTUM TRANSITION
X=0·07
X=0·09
X=0·15
ELECTROMETER READING ×2×10^14
(AMPERES)
RELATIVE R·F· AMPLITUDE

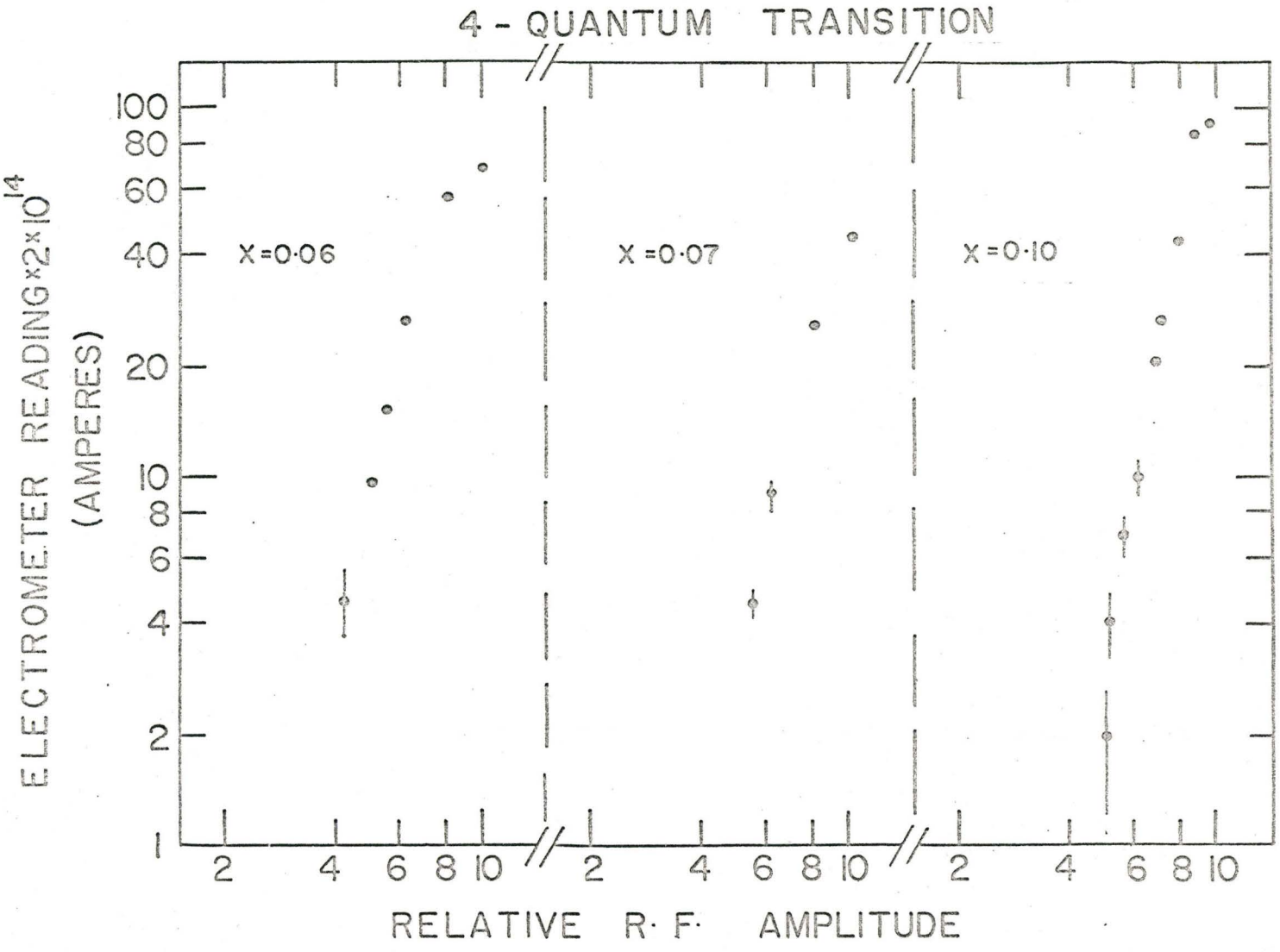
4 - QUANTUM TRANSITION
ELECTROMETER READING x 2 x 10^14 (AMPERES)
100
80
60
40
20
10
8
6
4
2
1
X = 0·06
X = 0·07
X = 0·10
2
4
6
8
10
RELATIVE R·F· AMPLITUDE

from one another. The shape of the power dependence curves appears to be determined solely by transition multiplicity.

When plotted in the manner of Figures 10, the experimental points can be fairly well fitted by a straight line for transition intensities between about 5 and 75 % of the maximum transition intensity. The implication of this observation is that for $b < b_{opt}$, the MQT transition intensity I is approximately given by $I \simeq b^c$. For those experiments, c was found to be about 1.7, 3.5, 4.3 and 5.5 for the 1, 2, 3 and 4-quantum transitions respectively.

Figures 11 show the power dependence results of the MQT theory developed in Section (III-5). These results are presented as curves which are fitted to the experimental points.

The curves were fitted to the experimental points by eye, using the following method. The computed power dependence curve and the experimental points were plotted on separate sheets of full logarithmic graph paper having the same scale. The graph of experimental points was taped down on a "light-box" and the graph of the calculated power dependence was adjusted horizontally and vertically until the best fit was obtained. An absolute requisite of this procedure was to keep the abscissas and ordinates of the two graphs parallel.

It was found to be impossible, or at least quite artificial, to fit, for example, a 4-quantum transition with the power dependence calculated for a 3-quantum transition. And it was definitely impossible, for example, to fit the 1 or 3-quantum experimental points with the 2 or 4-quantum calculated power dependence curves.

Figures 11a and 11b

Calculated Power Dependence Curves Fitted to Experimental Points

The 1 and 4-quantum experimental data are composite.

The values of x are:

1-quantum - $x = 0.18$

2-quantum - $x = 0.07$

3-quantum - $x = 0.07$

4-quantum - $x = 0.10$.

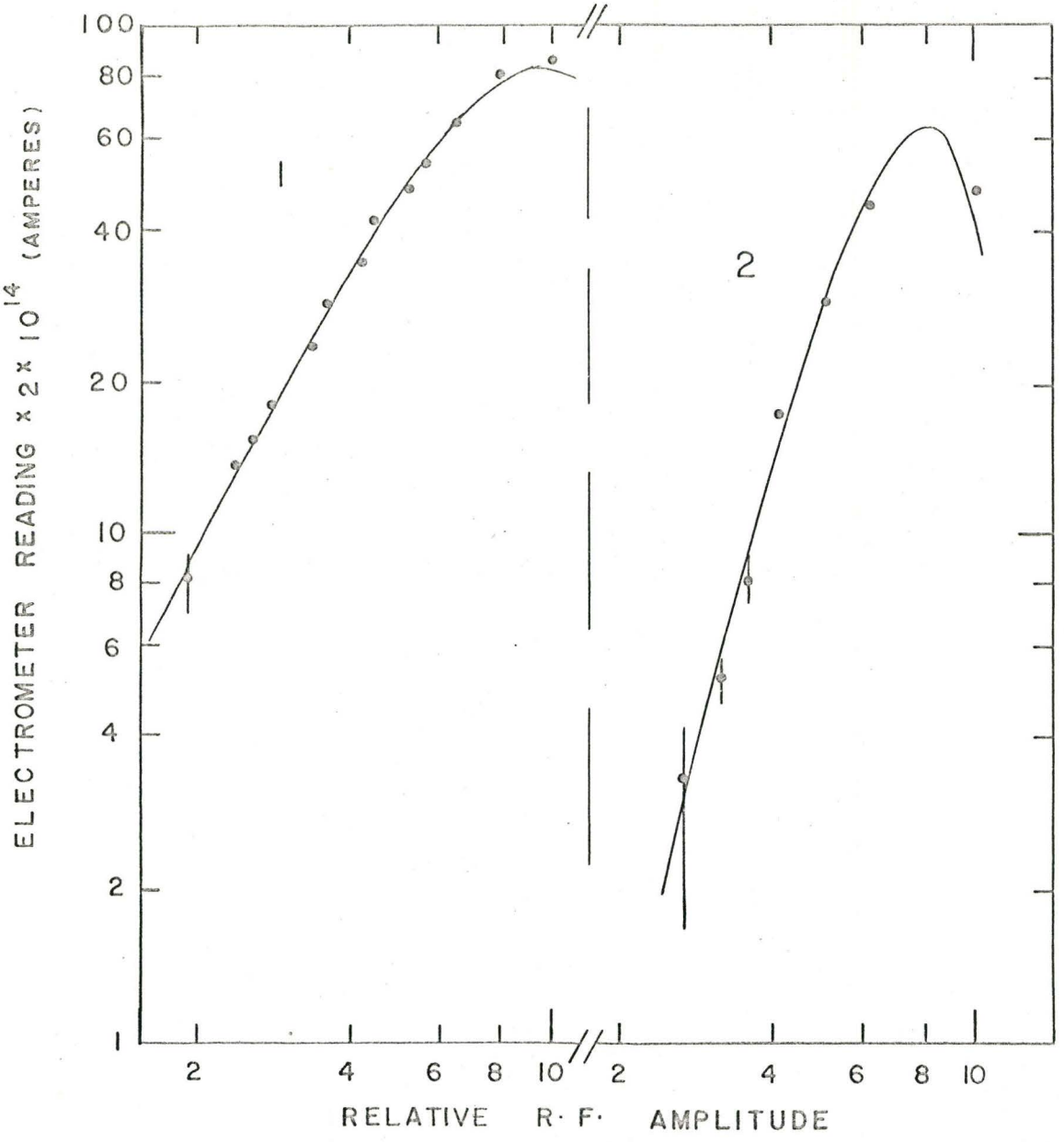
100
80
60
40
20
10
8
6
4
2
1
ELECTROMETER READING × 2 × 10^14 (AMPERES)
1
2
2
4
6
8
10
2
4
6
8
10
RELATIVE R·F· AMPLITUDE

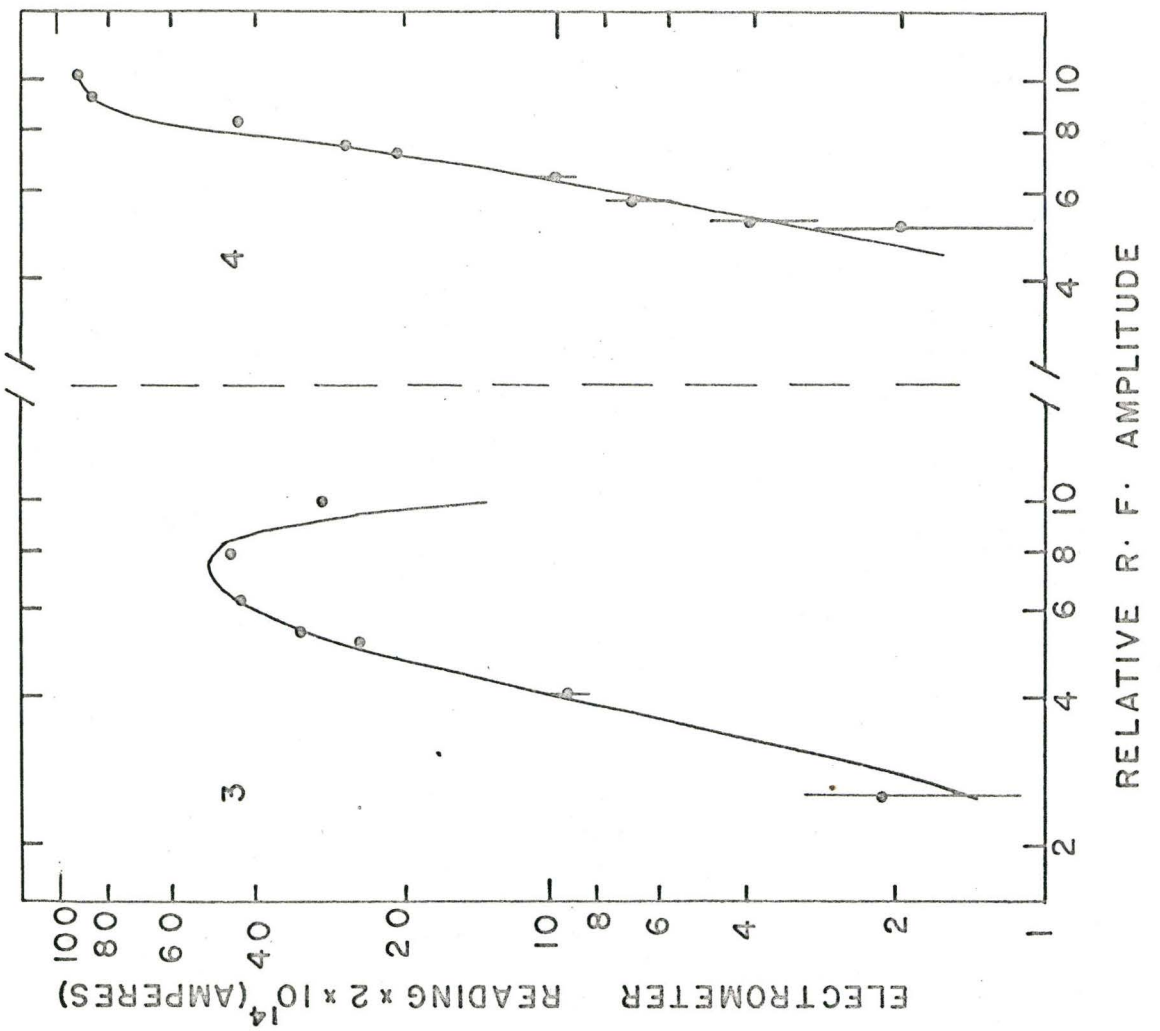
ELECTROMETER READING × 2 × 10^14 (AMPERES)
100
80
60
40
20
10
8
6
4
2
1
3
4
2
4
6
8
10
RELATIVE R. F. AMPLITUDE

Both the calculated and experimental power dependence curves showed no apparent dependence upon x. Hence, the experimental points were fitted by curves calculated near, but not necessarily at, the value of x at which the experiment was performed. In fact, for these values of x, the shapes of the Majorana curves (Figures 4) were indistinguishable from the shapes of the power dependence curves computed using the results of Section (III-5). Thus, an equally good fit would have resulted had the experimental points been fitted to the curves obtained from the Majorana formula.

Supplementary calculations, using the expressions developed in Section (III-5), were also performed for the three-level problem, F = 1. The spacing of the levels was made appropriate to atomic hydrogen at a field corresponding to x = 0.05. The shape of the power dependence curves for the 1 and 2-quantum transitions in the F = 1 system (i.e. in atomic hydrogen), were, practically speaking, identical to the shapes of the 1 and 2-quantum power dependence curves for the MQT of Na^{23}.

2. Additional Calculated Results

Figures 12 show the calculated MQT resonance line shapes at x = 0.15. The small subsidiary maxima evident are attributed to the transition probability calculation not being velocity averaged. Shifts in the resonance frequency away from nominal MQT resonance frequency can be clearly seen.

Figure 13 is a plot of amplitude required to effect optimum MQT probability at various values of x. The dramatic dependence of b_{opt} upon x is clearly demonstrated.

Figures 12a and 12b

Calculated Resonance Line Shapes at b_{opt}

The dashed verticle line indicates the nominal resonance frequencies. The small subsidiary maxima are attributed to not having velocity averaged the calculation. Here, $x = 0.15$.

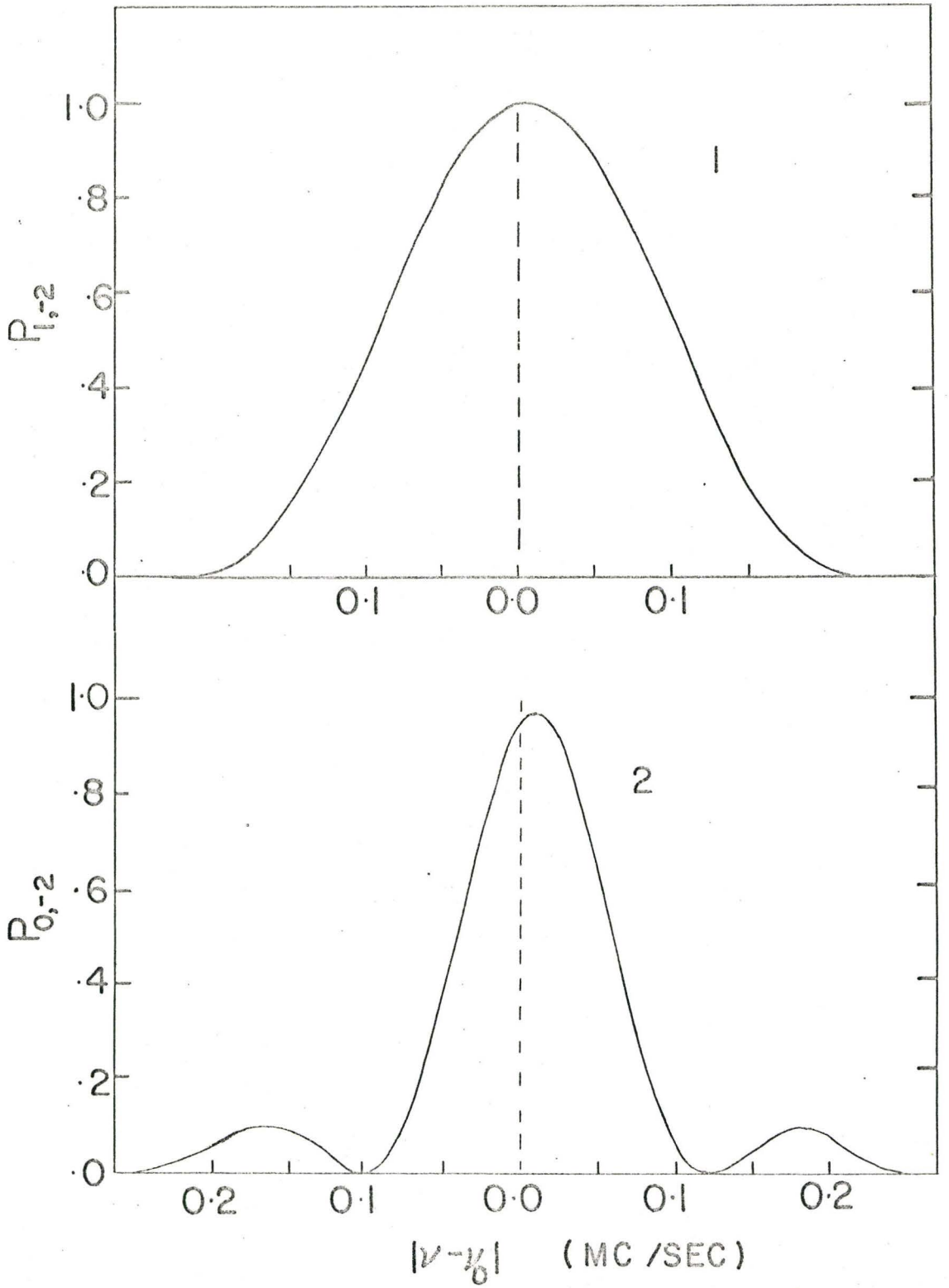
1·0
·8
·6
·4
·2
·0
$P_{1,-2}$
1
0·1
0·0
0·1
1·0
·8
·6
·4
·2
·0
$P_{0,-2}$
2
0·2
0·1
0·0
0·1
0·2
$|\nu-\nu_0|$ (MC/SEC)

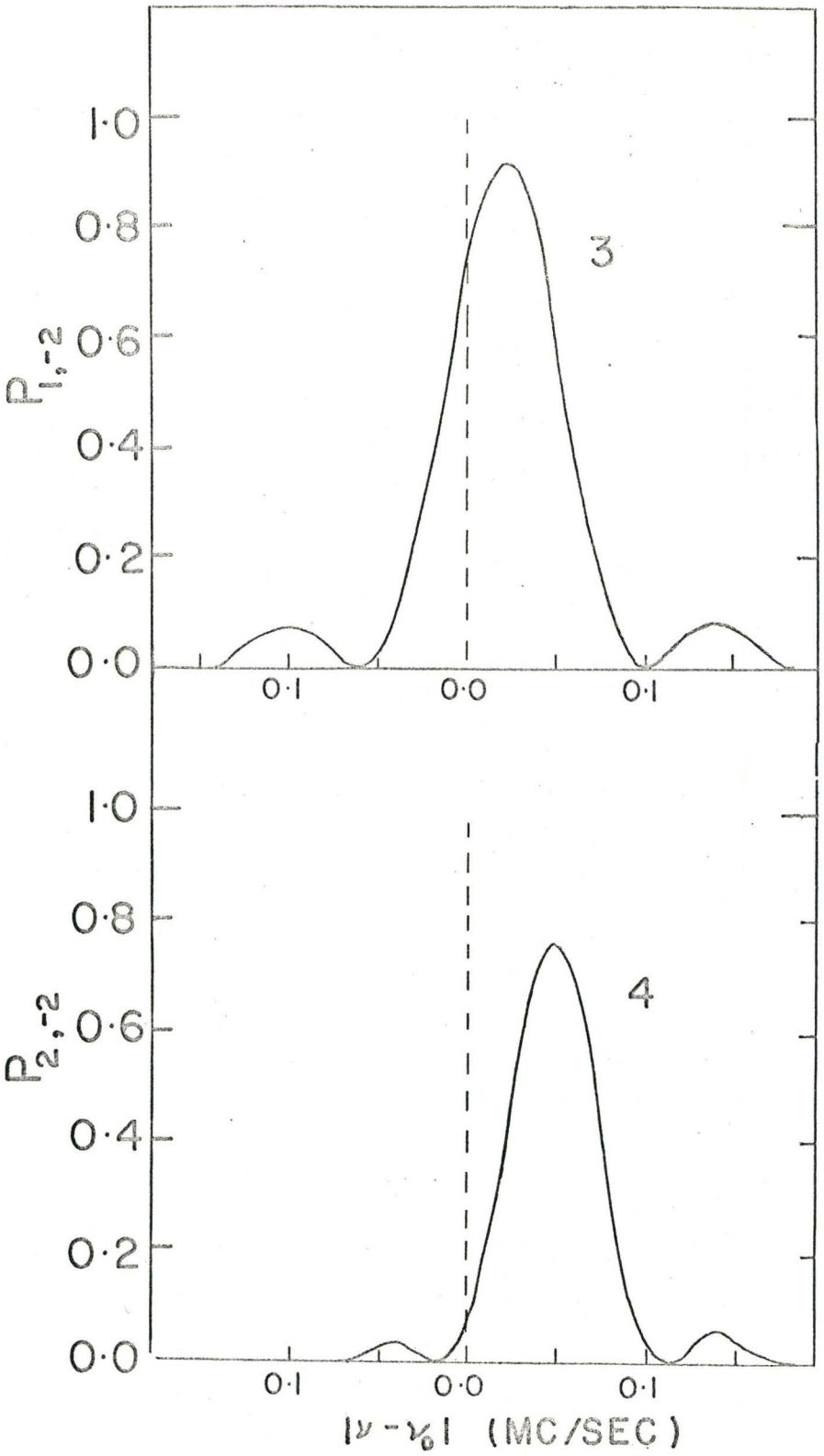
1·0
0·8
0·6
0·4
0·2
0·0
$P_{1,-2}$
3
0·1
0·0
0·1
1·0
0·8
0·6
0·4
0·2
0·0
$P_{2,-2}$
4
0·1
0·0
0·1
$|\nu - \nu_0|$ (MC/SEC)

Figure 13

Plot of b_{opt} vs. x

The dashed lines are to guide the eye.

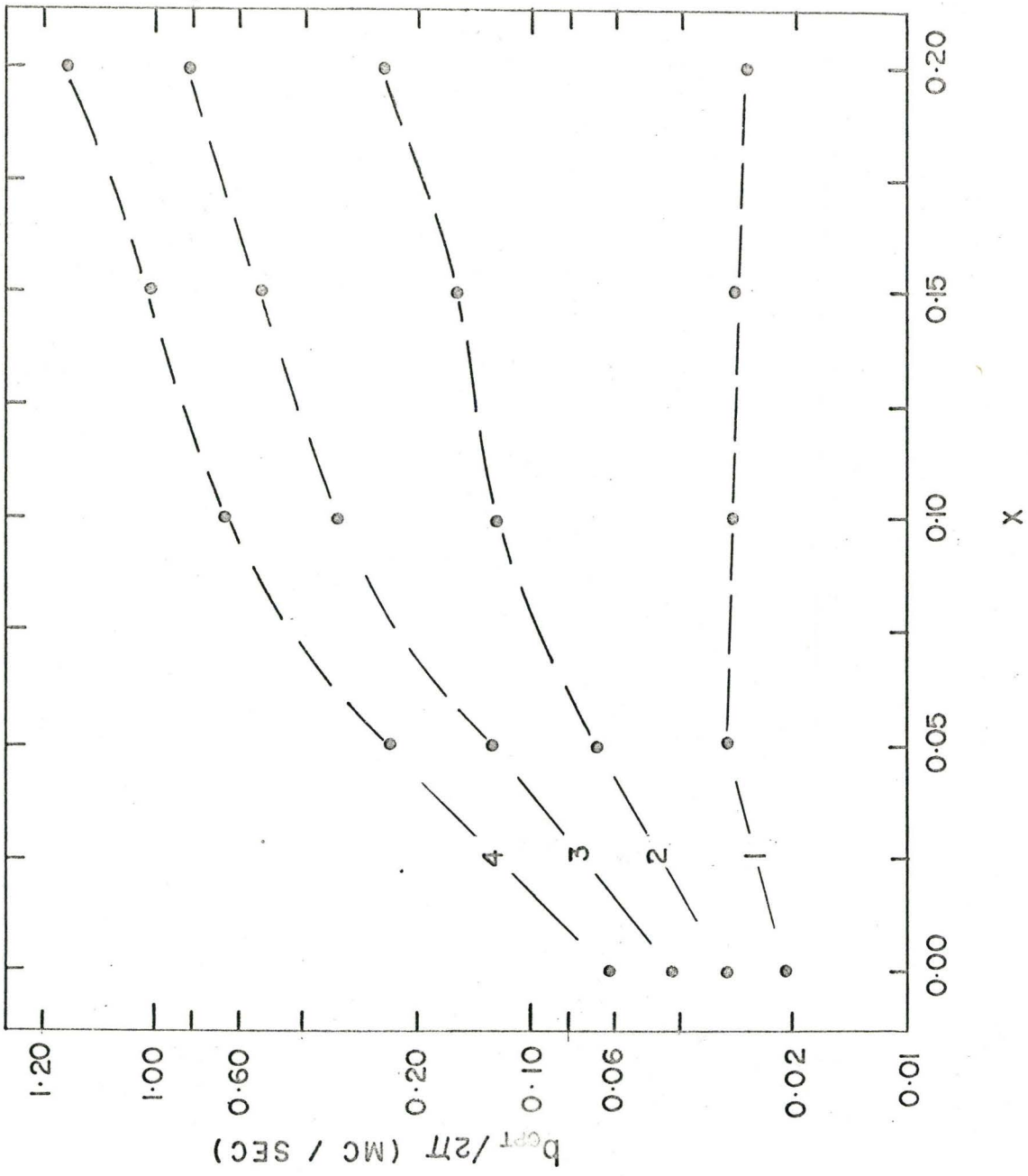
1·20
1·00
0·60
0·20
0·10
0·06
0·02
0·01
$b_{opt}/2\pi$ (MC / SEC)
0·00
0·05
0·10
0·15
0·20
X
1
2
3
4

Figures 14 are plots of the calculated shifts in resonance frequency for various values of b. It is seen that the shifts are approximately proportional to the square of the r.f. field amplitude.

Figure 15 gives the dependence of the FWHM upon x for optimum b. The value of t used is 4 microseconds. Using equation (3-28), $\Delta\nu \simeq \frac{1}{t} = \frac{1}{4 \times 10^{6} \text{ sec}} = 250$ kc/sec. It is seen that this is the FWHM for the 1-quantum transition in the equally spaced limit of $x = 0$. For $x > 0$, all of the FWHM decrease at different rates until, for larger values of x, they obey the $\frac{1}{n}$ law shown in Section (III-4).

Figures 14a and 14b

Calculated Frequency Shifts

For x = 0.025, no shift was observed in the 4-quantum transition for the values of b used.

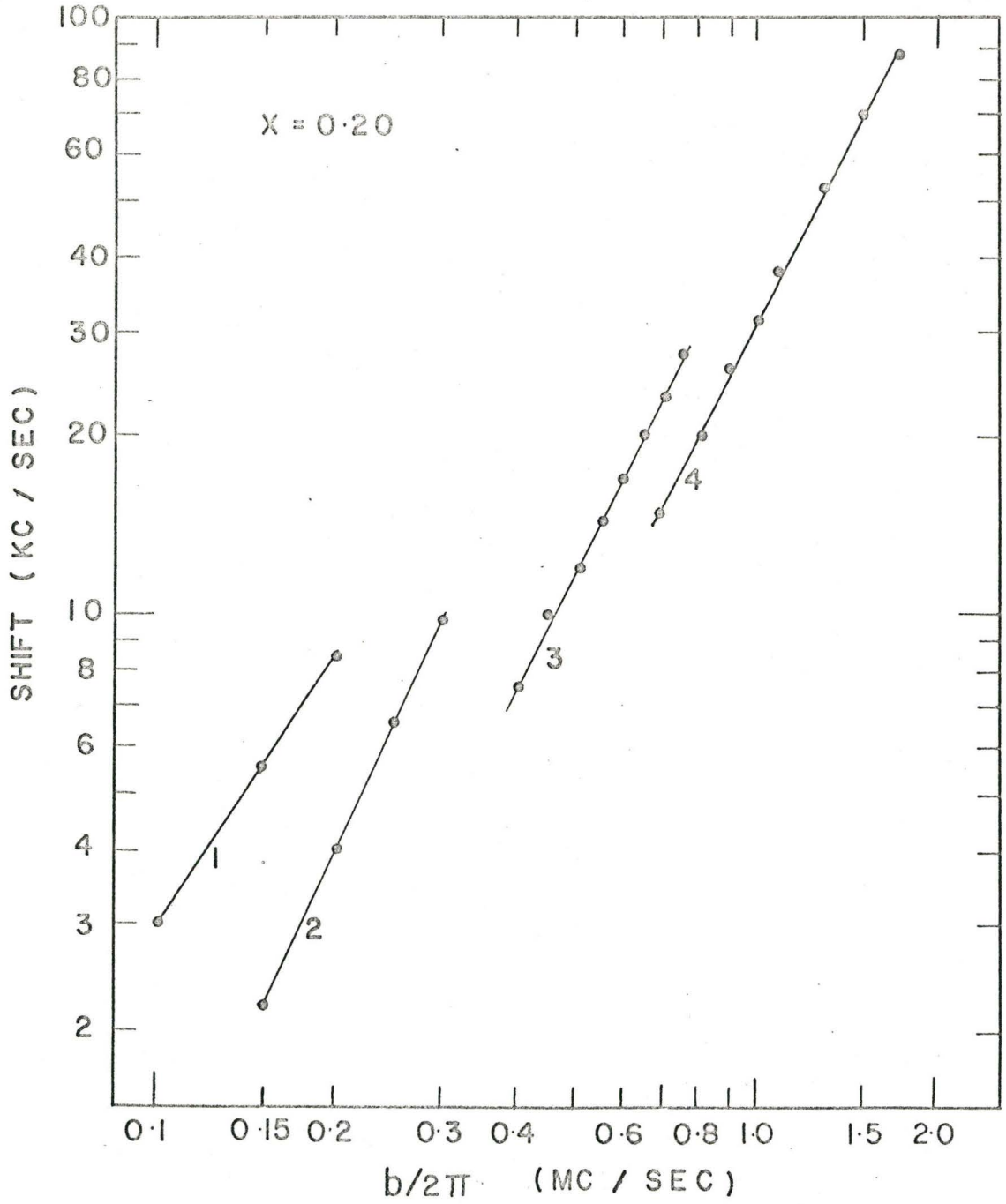
X = 0·20
SHIFT (KC / SEC)
100
80
60
40
30
20
10
8
6
4
3
2
1
2
3
4
0·1
0·15
0·2
0·3
0·4
0·6
0·8
1·0
1·5
2·0
b/2π (MC / SEC)

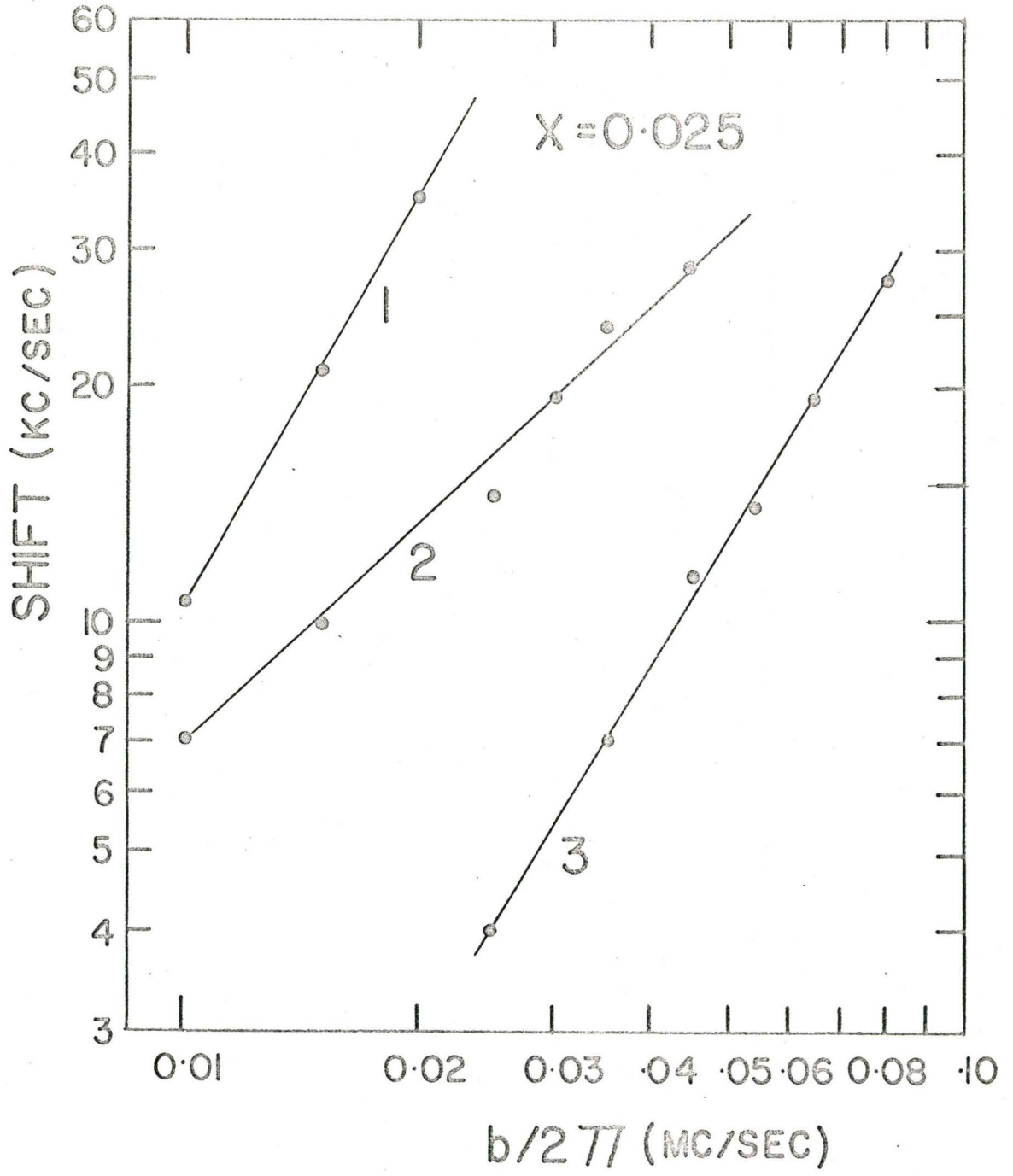
X=0·025
1
2
3
SHIFT (KC/SEC)
60
50
40
30
20
10
9
8
7
6
5
4
3
0·01
0·02
0·03
·04
·05
·06
0·08
·10
b/2π (MC/SEC)

Figure 15

Calculated FWHM

The lines drawn are to guide the eye.

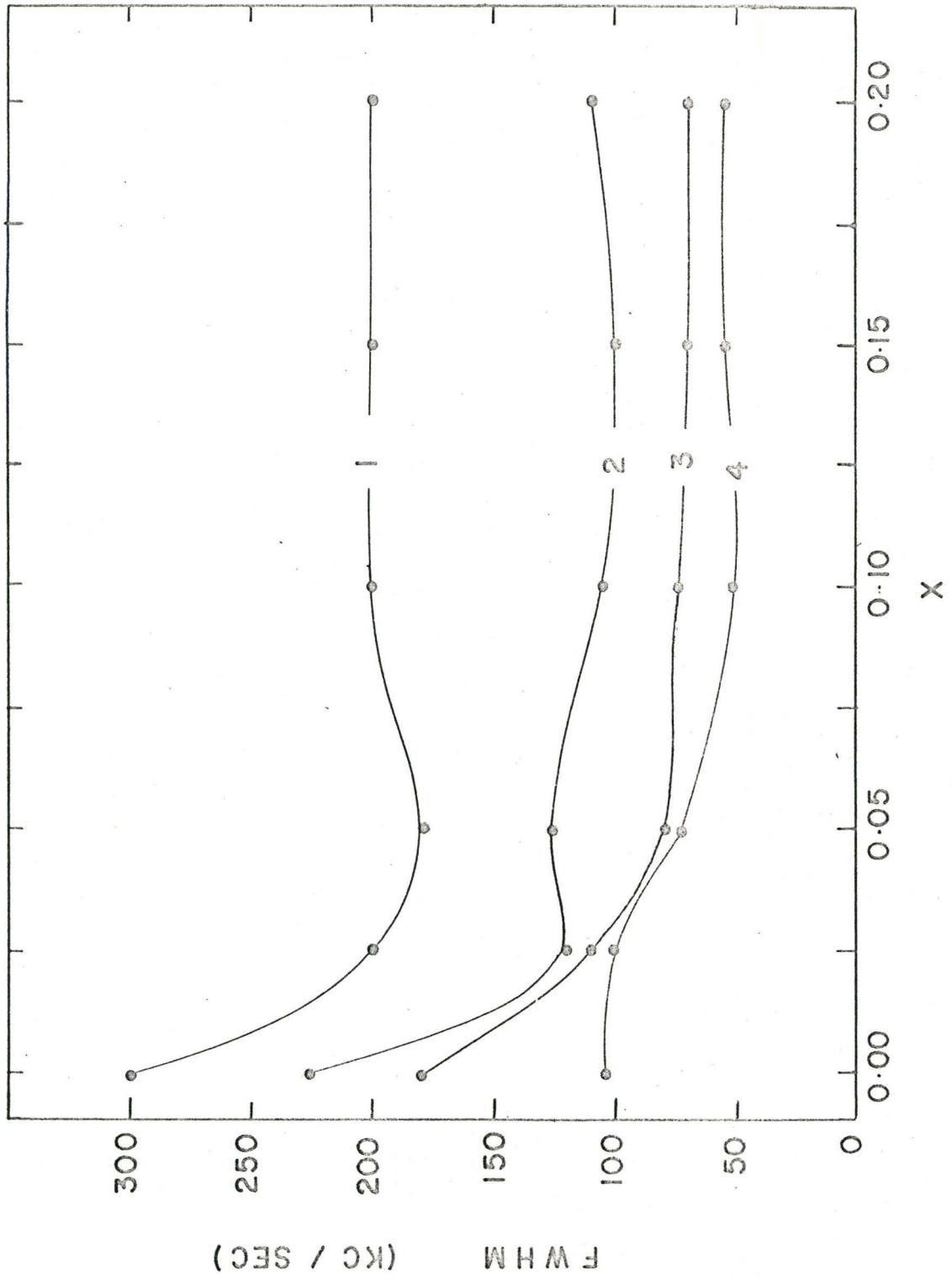
FWHM (KC / SEC)
300
250
200
150
100
50
0
0·00
0·05
0·10
0·15
0·20
X
1
2
3
4

CHAPTER VI

CONCLUSIONS

The results of the experiments and calculations performed indicate that the shape of the MQT power dependence curves is determined by transition multiplicity. One dividend of this result is the establishment of an experimental technique permitting the determination of transition multiplicity. The use of this technique may have broad application in ABMR.

The excellent agreement between the calculated and experimental power dependence curves establishes an important facet of the theory. For the well separated frequency case, agreement was obtained with aspects of the perturbation theory results of Salwen and Hack. These aspects were the 1/n behaviour of the FWHM of an n-quantum resonance line shape and the shift in resonance frequency which was shown to be quadratic in r.f. amplitude. In the zero field limit of exact equal spacing of the levels, the results of the theory developed in this work were identical to the results of the Majorana expression. Thus, there has been presented both experimental and theoretical verification of the theory. These results are felt to establish the validity of the calculations.

Ideally, the experiments reported here would have included measurements of the frequency shifts and the FWHM. Unfortunately, such measurements, using the McMaster apparatus, were practically impossible

due to inhomogeneities of the C field. There are, however, two additional experiments which should be feasible using the present apparatus. The first of these would be to ascertain the relative r.f. amplitudes required to optimize the transition intensity. This would form a test of the results presented in Figure 13. Naturally, the results of this experiment would have to be interpreted in the light of the assumption that the r.f. field is of uniform amplitude over its extent. Kusch attributes the unpredicted behaviour of MQT that he observed in K^{39} at large values of r.f. amplitude to this assumption. The second experiment would involve studying the MQT power dependence curves for hyperfine structures which have several hyperfine multiplets. This experiment would test the severity of neglecting hyperfine multiplets other than those in which the MQT were effected. An example of such MQT is the 2-quantum transition in Sm^{153} $J = 2$, $\left| \frac{3}{2}, -\frac{1}{2} \right\rangle \leftrightarrow \left| \frac{3}{2}, \frac{3}{2} \right\rangle$. This 2-quantum transition was observed at this laboratory by Eastwood.

In summary, a technique which aids the identification of transition multiplicity has been developed. Also, the results of a new theory of MQT have been presented.

BIBLIOGRAPHY

Breit, G. and Rabi, I. I. 1931. Phys. Rev. 38, 2082.

Cameron, J. A., King, H. J., Eastwood, H. K., and Summers-Gill, R.G. 1962. Can. J. Phys. 40, 931.

Eastwood, H. K. 1962. Ph.D. Thesis McMaster University.

Franzen, W. and Alam, M. 1964. Phys. Rev. 133, A460.

Hack, N. M. 1956. Phys. Rev. 104, 84.

King, H. J. 1960. Ph.D. Thesis McMaster University.

Kusch, P. 1956. Phys. Rev. 101, 627.

Majorana, E. 1932. Nuovo Cimento 9, 43.

Messiah, A. 1961. Quantum Mechanics (North Holland Publishing Company).

Rabi, I. I. 1937. Phys. Rev. 51, 652.

Rabi, I. I., Ramsey N. F., and Schwinger, J. 1954. Rev. Mod. Phys. 26, 167.

Ramsey, N. F. 1956. Molecular Beams (Oxford University Press).

Stinson, G. M. 1966. Ph.D. Thesis McMaster University.

Salwen, H. 1955. Phys. Rev. 99, 1274.

Salwen, H. 1956. Phys. Rev. 101, 623.